Study on energy transfer of dyes and metal complexes introduced into DNA structures

(DNA 構造体に導入した色素および金属錯体のエネルギー移動に関する研究)

AZUMA Hidenori

東 秀憲

2024

Table of contents

Capter 1 Development of light harvesting system using DNA with multiple fluorophores (Förster energy transfer between fluorophores)

1-1 Energy transfer

Excitation energy transfer (ET), in which excitation energy is transferred from one excited molecule to another, is a very important phenomenon in light-emitting materials, photosynthesis, and photocatalysis. ET can be divided into two types: singlet-singlet energy transfer (SSET), in which energy is transferred from a singlet excited donor to form a singlet excited acceptor, and triplet-triplet energy transfer (TTET), in which energy is transferred from a triplet excited donor to form a triplet excited acceptor.

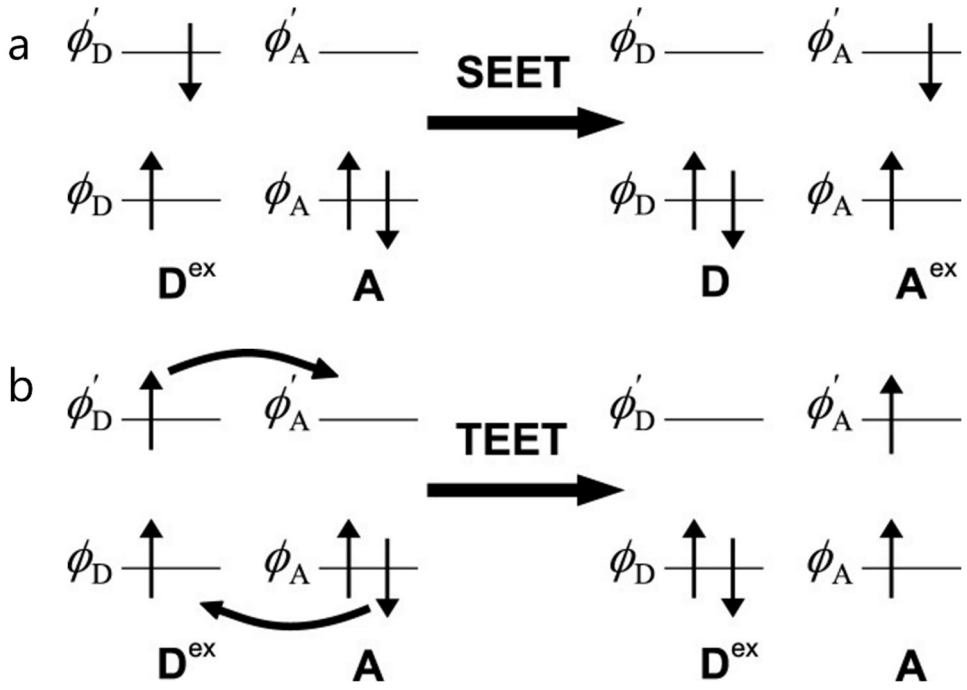

Figure 1-1. Simplified four-orbital scheme for (a) SEET and (b) TEET. Reprinted from Ref. 1.

ET generally proceeds according to either Förster theory [2] or Dexter theory [3]. In Förster theory, excitation energy is transferred by electron resonance and only SSET is possible. ET according to Förster theory requires an overlap between the emission spectrum of the donor and the absorption spectrum of the acceptor, and depend on the distance and orientation between dyes. In Dexter theory, excitation energy is transferred by electron exchange and both SSET and TTET

are possible. ET according to Dexter theory requires an orbital overlap. Due to distance-dependence of ET, molecules must be spatially precisely aligned to control ET.

1-2 DNA

Deoxyribonucleic acid (DNA) is a biopolymer that stores the genetic information of living organisms and is the most famous and important biomolecule. The building blocks of DNA are nucleotides composed of deoxyribose, bases, and phosphates. There are four types of nucleobases in DNA: adenine (A), cytosine (C), guanine (G), and thymine (T). The nucleobases recognize each other in structure, forming A-T base pair with two hydrogen bonds and G-C base pair with three hydrogen bonds. This base pairing is called Watson-Crick base pairing. Using this base pairing formation, DNA with complementary sequences form rigid right-handed double helix with excellent sequence selectivity. Triples and quadruplexes can also be formed by using Hoogsteen base pairing formation.DNA with special sequences forms more complex structures such as Holliday junctions.

This sequence-selective duplex formation is very important for biological systems. Since Watson and Crick revealed the structure of DNA in 1953[4], its unique functions have been revealed and applied to numerous types of systems.

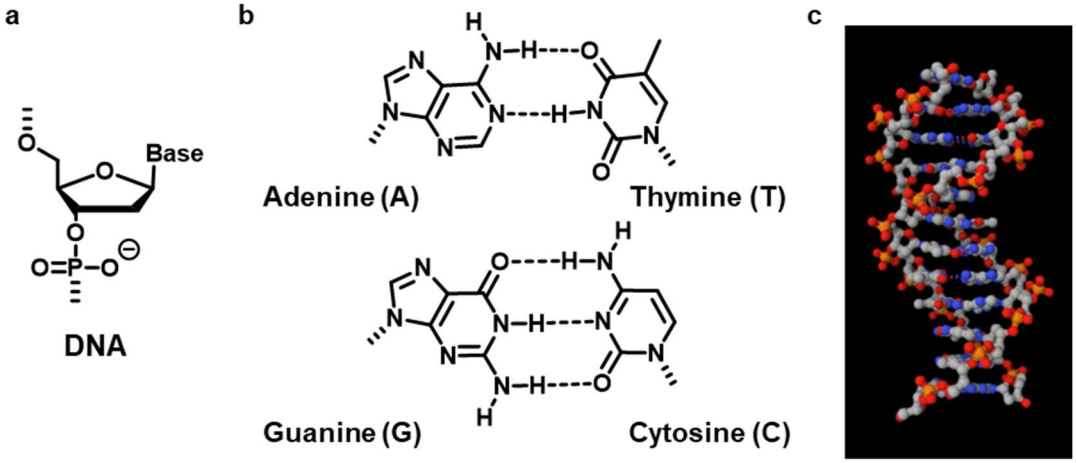

Figure 1-2. (a) Chemical structure of nucleotide. (b) Chemical structure of Watson-Crick base pair. (c) Structure of DNA duplex.

1-3 DNA nanotechnology

DNA has a unique function of sequence-selective structure formation based on base pairing. as a nanomaterial. The structure is easily predicted from the DNA sequence. The development of chemical synthesis of DNA has realized DNA nanotechnology. The foundation for DNA nanotechnology was laid by Seaman in the 1980s. Two-dimensional lattices and three-dimensional cubes were created by the self-assembly of designed DNA [5].

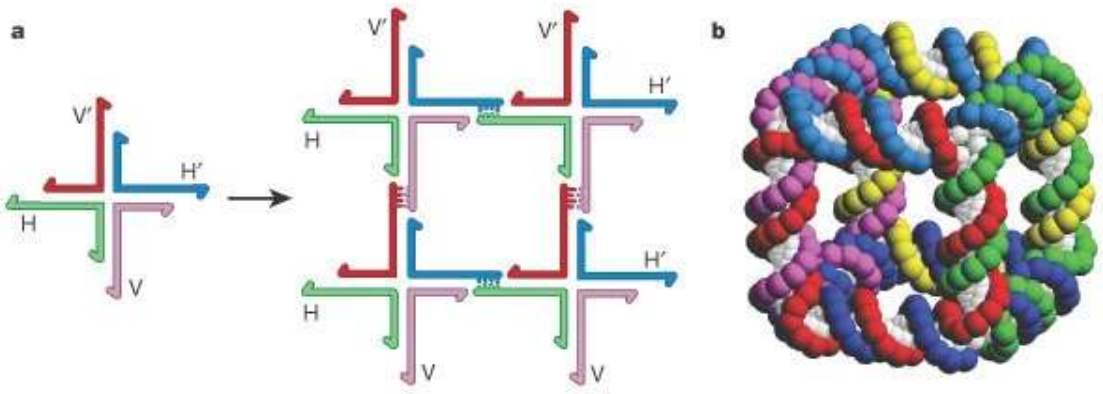

Figure 1-3. Schematic illustrations of (a) two-dimensional DNA lattices and (b) three-dimensional DNA cube. Reprinted from Ref. 5.

DNA origami [6] is the most important and central research subject in the field of DNA nanotechnology. A single strand of DNA longer than 7,000 bases, called the scaffold strand, is folded with more than 200 shorter DNA strands, called staple strands. By designing the staple chain sequence, the folding chain folds into the desired shape, such as a star or smiley.

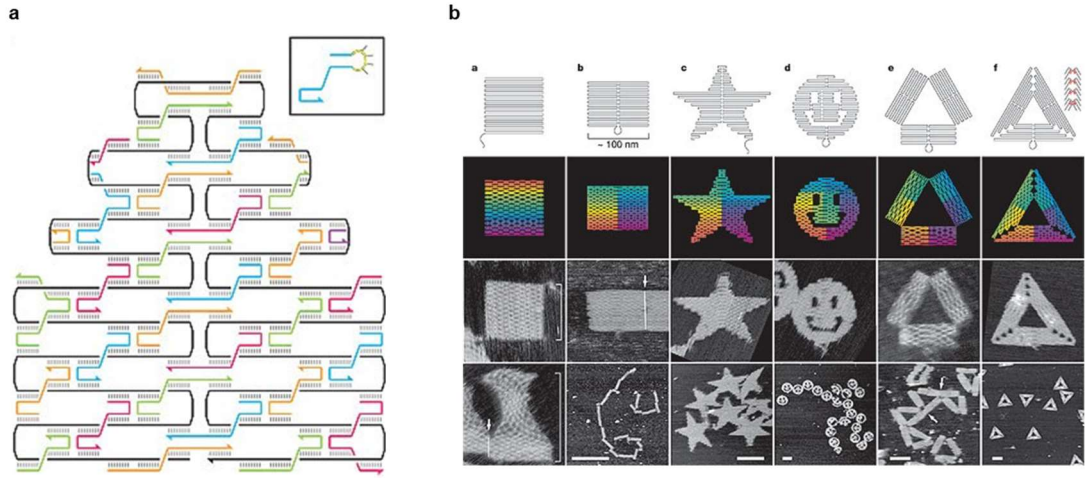

Figure 1-4. (a) Schematic illustrations of DNA origami. (b) AFM images of DNA origami folded into desired shape. Reprinted from Ref. 6.

Dynamic DNA nanotechnologies such as DNA tweezers [7], DNA walkers [8], and DNA logic gates [8] are also being developed. These DNA nanotechnologies are an innovative technology that allows the free design and creation of nanoscale structures using only self-assembly.

Various types of functionalized DNA nanostructures have been developed because DNA is easily modified with functional molecules. DNA origami has been extended to three dimensions and applied to nanoreactor [9 10] and drug delivery systems [11 12]. Thus, DNA can be used as a scaffold

for various types of systems and has many possibilities to develop biological and chemical nanodevices.

1-4 Excitation energy transfer control using DNA as a backbone

DNA is an ideal backbone for the study of excitation energy transfer. Various types of dyes can be easily placed in the rigid DNA nanostructures formed by the designed sequences. One-step ET systems been developed by using DNA as a backbone [13] [14].

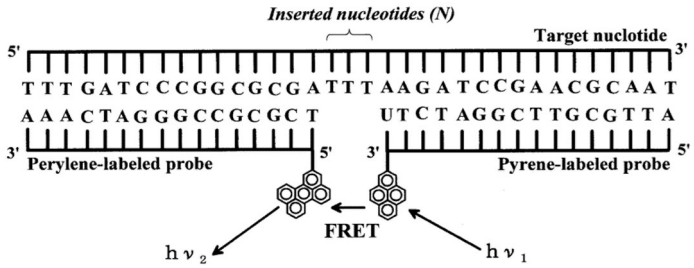

Figure 1-5. One-step ET system using DNA as a backbone. Reprinted from Ref. 13.

Our laboratory has reported orientation-dependent FRET systems by using D-threoninol [15] [16]. Dye introduced into the DNA duplex via D-threoninol is intercalated between natural base pairs and orientation is fixed [17] FRET systems between homologous dyes (homo-FRET) were developed as well[18]. In these systems, ET strictly followed Förster theory.

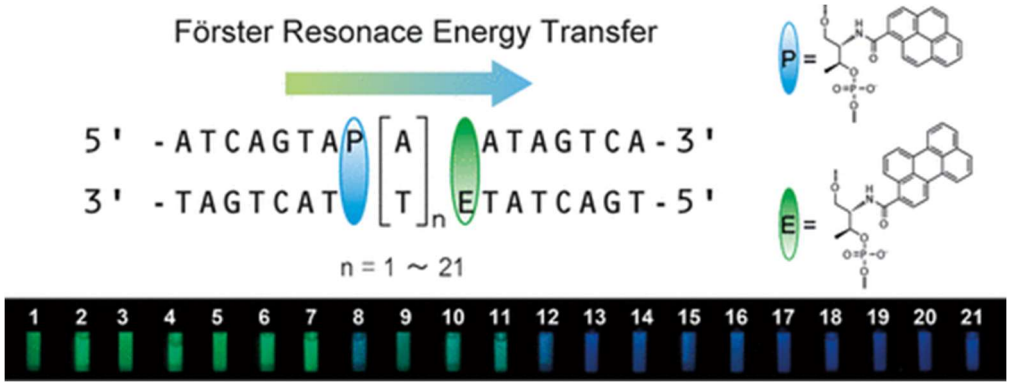

Figure 1-5. orientation-dependent FRET system. Reprinted from Ref. 15.

Not only one-step FRET but also multi-step FRET systems have been developed [19] [20]. Multiple dyes are spatially precisely arranged, and excitation energy is transferred in turn from dyes with higher excitation energy to those with lower excitation energy. Removal of the intermediate dyes interrupt the excitation energy transfer.

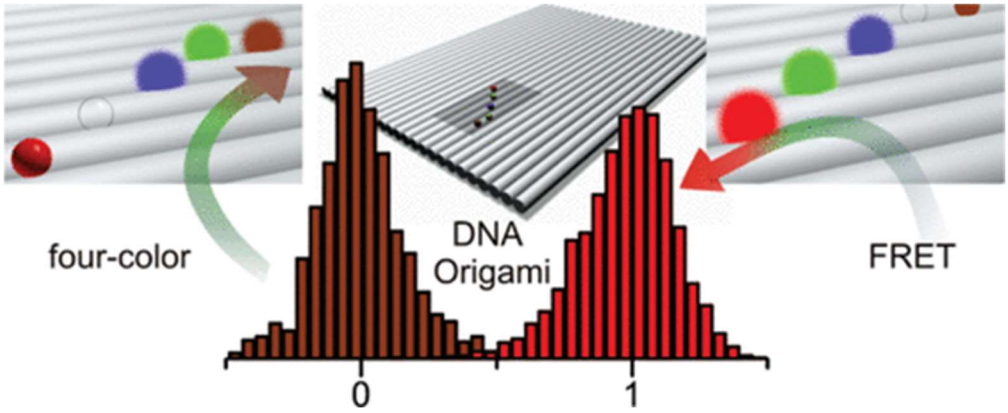

Figure 1-6. Multi-step FRET system using DNA origami as a backbone. Reprinted from Res. 19.

Further functionalization is possible by simultaneously integrating molecules such as gold nanoparticles [21] and proteins[22].

1-5 Purpose of this study

In this study, we developed energy transfer systems for dyes and metal complexes introduced into DNA structures. In Chapter 2, We developed light-harvesting antennas with multiple dyes accumulated in DNA junctions for the application using Förster energy transfer from dye to dye. In Chapter 3, we developed a molecular ruler that depends only on distance. using Förster energy transfer from metal complex to dye. In Chapter 4, we developed visible light cross-linking system for DNA duplexes catalyzed by metal complex using Dexter energy transfer from metal complex to dye.

1-6 References

1. You, Z.-Q.; Hsu, C.-P., Theory and calculation for the electronic coupling in excitation energy transfer. *International Journal of Quantum Chemistry* **2014,** *114* (2), 102-115.

2. Förster, T., Zwischenmolekulare Energiewanderung und Fluoreszenz. *Annalen der Physik* **1948,** *437* (1-2), 55-75.

3. Dexter, D. L., A Theory of Sensitized Luminescence in Solids. *The Journal of Chemical Physics* **1953,** *21* (5), 836-850.

4. Watson, J. D.; Crick, F. H. C., Molecular Structure of Nucleic Acids: A Structure for Deoxyribose Nucleic Acid. *Nature* **1953,** *171* (4356), 737-738.

5. Seeman, N. C., DNA in a material world. *Nature* **2003,** *421* (6921), 427-431.

6. Rothemund, P. W. K., Folding DNA to create nanoscale shapes and patterns. *Nature* **2006,** *440* (7082), 297-302.

7. Yurke, B.; Turberfield, A. J.; Mills, A. P.; Simmel, F. C.; Neumann, J. L., A DNA-fuelled molecular machine made of DNA. *Nature* **2000,** *406* (6796), 605-608.
8. Shin, J.-S.; Pierce, N. A., A Synthetic DNA Walker for Molecular Transport. *Journal of the American Chemical Society* **2004,** *126* (35), 10834-10835.
9. Grossi, G.; Dalgaard Ebbesen Jepsen, M.; Kjems, J.; Andersen, E. S., Control of enzyme reactions by a reconfigurable DNA nanovault. *Nature Communications* **2017,** *8* (1), 992.
10. Tokura, Y.; Harvey, S.; Xu, X.; Chen, C.; Morsbach, S.; Wunderlich, K.; Fytas, G.; Wu, Y.; Ng, D. Y. W.; Weil, T., Polymer tube nanoreactors via DNA-origami templated synthesis. *Chemical Communications* **2018,** *54* (22), 2808-2811.
11. Douglas, S. M.; Bachelet, I.; Church, G. M., A Logic-Gated Nanorobot for Targeted Transport of Molecular Payloads. *Science* **2012,** *335* (6070), 831-834.
12. Takenaka, T.; Endo, M.; Suzuki, Y.; Yang, Y.; Emura, T.; Hidaka, K.; Kato, T.; Miyata, T.; Namba, K.; Sugiyama, H., Photoresponsive DNA Nanocapsule Having an Open/Close System for Capture and Release of Nanomaterials. *Chemistry – A European Journal* **2014,** *20* (46), 14951-14954.
13. Masuko, M.; Ohuchi, S.; Sode, K.; Ohtani, H.; Shimadzu, A., Fluorescence resonance energy transfer from pyrene to perylene labels for nucleic acid hybridization assays under homogeneous solution conditions. *Nucleic Acids Research* **2000,** *28* (8), e34-00.
14. Hurley, D. J.; Tor, Y., Donor/Acceptor Interactions in Systematically Modified RuII−OsII Oligonucleotides. *Journal of the American Chemical Society* **2002,** *124* (44), 13231-13241.
15. Kato, T.; Kashida, H.; Kishida, H.; Yada, H.; Okamoto, H.; Asanuma, H., Development of a Robust Model System of FRET using Base Surrogates Tethering Fluorophores for Strict Control of Their Position and Orientation within DNA Duplex. *Journal of the American Chemical Society* **2013,** *135* (2), 741-750.
16. Kawai, H.; Doi, T.; Ito, Y.; Kameyama, T.; Torimoto, T.; Kashida, H.; Asanuma, H., Perylene-Cy3 FRET System to Analyze Photoactive DNA Structures. *Chemistry – A European Journal* **2021,** *27* (50), 12845-12850.
17. Fujii, T.; Kashida, H.; Asanuma, H., Analysis of Coherent Heteroclustering of Different Dyes by Use of Threoninol Nucleotides for Comparison with the Molecular Exciton Theory. *Chemistry – A European Journal* **2009,** *15* (39), 10092-10102.
18. Kashida, H.; Kawai, H.; Azuma, H.; Araki, Y.; Wada, T.; Asanuma, H., Quantitative Analyses of Förster Resonance Energy Transfer between Identical Pyrene Chromophores (Homo-FRET) In DNA Scaffolds. *ChemPhotoChem* **2021,** *5* (2), 167-172.
19. Stein, I. H.; Steinhauer, C.; Tinnefeld, P., Single-Molecule Four-Color FRET Visualizes Energy-Transfer Paths on DNA Origami. *Journal of the American Chemical Society* **2011,** *133*

(12), 4193-4195.

20. Dutta, P. K.; Varghese, R.; Nangreave, J.; Lin, S.; Yan, H.; Liu, Y., DNA-Directed Artificial Light-Harvesting Antenna. *Journal of the American Chemical Society* **2011,** *133* (31), 11985-11993.

21. Aissaoui, N.; Moth-Poulsen, K.; Käll, M.; Johansson, P.; Wilhelmsson, L. M.; Albinsson, B., FRET enhancement close to gold nanoparticles positioned in DNA origami constructs. *Nanoscale* **2017,** *9* (2), 673-683.

22. Dutta, P. K.; Levenberg, S.; Loskutov, A.; Jun, D.; Saer, R.; Beatty, J. T.; Lin, S.; Liu, Y.; Woodbury, N. W.; Yan, H., A DNA-Directed Light-Harvesting/Reaction Center System. *Journal of the American Chemical Society* **2014,** *136* (47), 16618-16625.

Capter 2 Development of light harvesting system using DNA with multiple fluorophores (Förster energy transfer from dye to dye)

2-1 Abstract

We developed a novel light harvesting system using DNA junction for high-density accumulation of fluorophores. The fluorophores were accumulated via D-threoninol so that interactions between the fluorophores are strictly controlled. Highly efficient collection of light energy from the pyrene integrated in the arms of the DNA junction to the perylene placed in the center of the DNA junction. A large amount of light energy is efficiently transferrd from the pyrene integrated in the arms of the DNA junction to the perylene placed in the center of the DNA junction. Antenna effects of 3-way to 8-way junction were compared. Interestingly, the antenna effects of even-numbered junction were higher than that of odd-numbered junction. As a result, the antenna effects of 6- way and 8-way junction are the highest, and their effective absorption coefficients were 8.5 times higher than the absorption coefficient of perylene. The yield of even-numbered junction was found to be higher than that of odd-numbered junction from native-PAGE. This system can be used for high brightness labeling agents and artificial photosynthesis systems.

2-2 Introduction

Natural photosynthesis is a photochemical phenomenon that converts light energy into chemical energy with ultra-high efficiency. Photosynthesis achieves highly efficient light-harvesting by integrating a large number of pigments by strictly controlling their distance and orientation and optimizing the flow of energy. After many dyes absorb light energy, the energy is transferred between dyes, and finally to the reaction center without any energy loss, resulting in highly efficient light harvesting [1]. Artificial photosynthesis, which mimics this photosynthesis, is being studied challengingly from the perspective of clean energy acquisition. Artificial photosynthetic systems based on coordinate bonds [2] and covalent bonds [3] have been reported. To achieve highly efficient energy transfer, not only the distance between dyes but also their orientation must be strictly controlled. Generally, it is difficult to control the orientation between dyes.

DNA is the ideal backbone for precise integration of dyes. Various types of dyes can easily be introduced via covalent bonding to DNA. DNA spontaneously forms rigid duplexes and can form a variety of complex structures by designing the sequence, allowing precise integration of dyes. Various light harvesting antennas have been developed using multi branched DNA structures as backbone [4 5 6]. Within these antennas, light energy is transferred between dyes by multistep Förster

resonance energy transfer (FRET). In these systems, it is difficult to control the orientation between dyes and achieve high-density accumulation.

Our laboratory has reported a FRET system with strict control of orientation as well as distance by using D-threoninol [7] [8]. Dye introduced into the DNA duplex via D-threoninol is intercalated between natural base pairs and orientation is fixed [9].

In this study, we developed a novel light harvesting system using DNA junction. D-threoninol was used for high-density accumulation of multiple fluorophores into the DNA junction. The orientation between fluorophores as well as the distance is strictly controlled, so highly efficient light collection can be expected.

2-3 Design

Conventional systems using DNA duplexes are limited in the number of dyes that can be introduced, which limits the achievable light-harvesting capacity. In order to further increase the number of dyes introduced, DNA junction, a higher-order structure of DNA, was adopted as the backbone of the light-harvesting system. A DNA junction is a multi-branched structure consisting of multiple DNA duplexes connected at junction sites. In general, it is known that the closer the distance between dyes, the more highly efficient the energy transfer. The number of energy transfer donors that can be placed near energy transfer acceptors can be increased by using DNA junctions. Specifically, multiple molecules of pyrene, a donor for energy transfer, were introduced into the duplex site of the DNA junction, and a molecule of perylene, an acceptor for energy transfer, was introduced into the junction site. The design is shown in Fig. 2-1. This design allows a large number of pyrenes to absorb light energy, which then transfers energy among the pyrenes and eventually to the perylene. In other words, highly efficient light harvesting can be expected, similar to natural photosynthesis.

The predecessor optimized the following dye configurations using normal duplex DNA.

- Distance between pyrenes

The shorter the distance between pyrenes, the better the energy transfer efficiency. However, when pyrenes are adjacent to each other, excimer is formed. When the distance between the pyrenes is 1 mer, quenching due to dye-dye interactions occurs, which is inappropriate. Based on the above, the optimal distance between pyrenes is 2 mer.

- Distance between pyrene and perylene

The shorter the distance between pyrene and perylene, the better the energy transfer efficiency. However, both sides of the dye must be adenine or thymine to prevent quenching by guanine. In addition, sufficient chain length is required for stable formation of junction. Based on the above, the optimal distance between pyrene and perylene is 6 mer.

- Number of pyrene in each arm

Comparing pyrene numbers from 5 to 7 mer, the energy transfer efficiency was 5 mer < 6 mer = 7 mer. This is due to the fact that the seventh and later pyrenes counted from the perylene side are too far away from perylene for energy transfer to occur. Therefore, the optimal number of pyrene in one arm is 6 mer.

The DNA sequences of the 3-way to 8-way junction designed from the above optimization conditions are shown in Fig. S2-3. DNA junction with acceptor is designed to form a junction by mixing equal amounts of E and number sequences, and DNA junction without acceptor is designed to form a junction by mixing equal amounts of N and number sequences.

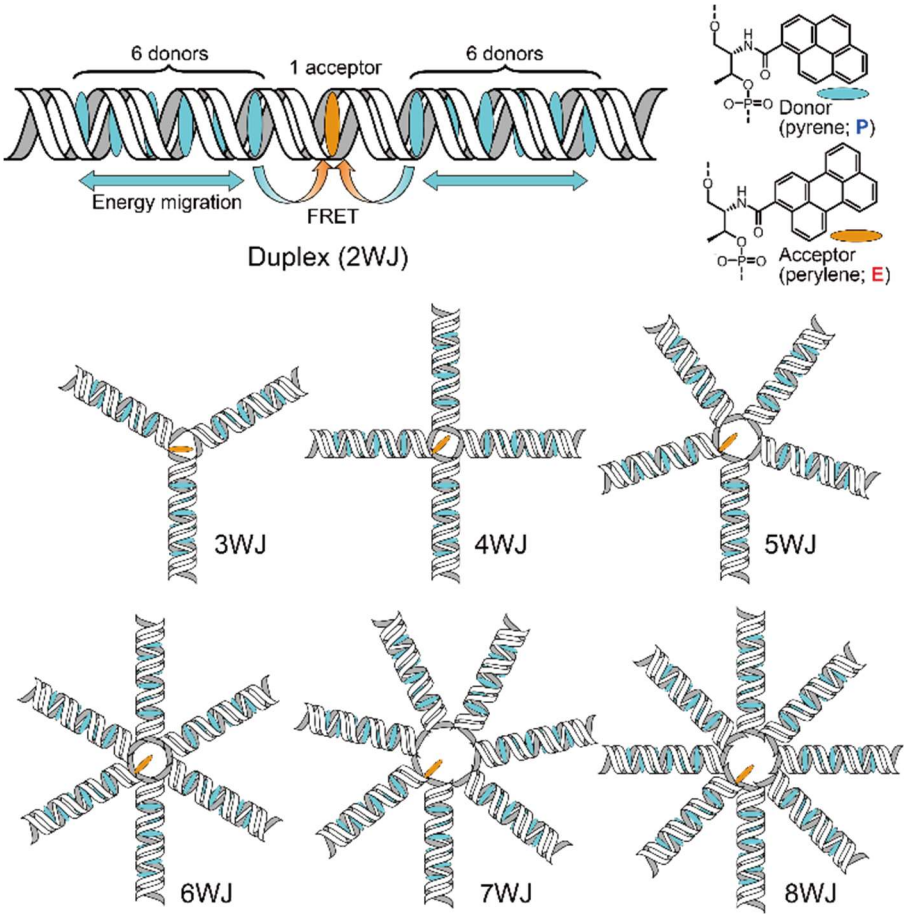

Figure 2-1. Illustration and design of DNA junctions prepared in this study.

2-4 Results and discussions

2-4-1 Antenna effect evaluation methods

The effective absorption coefficient was used as a method to evaluate the antenna effect. The effective absorption coefficient ($\varepsilon_{\mathrm{eff}}$) is calculated from the following equation.

$$\varepsilon_{\mathrm{eff}} = \varepsilon_{\mathrm{D}} \Phi_{\mathrm{T}}$$

Where ε_{D} is the absorption coefficient of donors, and Φ_{T} is the FRET efficiency. Absorption coefficient of donors and FRET efficiency are calculated from the following equation.

$$\varepsilon_{\mathrm{D}} = \frac{A_{\mathrm{D}}}{c\,l}$$

$$\Phi_{\mathrm{T}} = 1 - \frac{I_{\mathrm{DA}}}{I_{\mathrm{D}}}$$

Where A_{D} is the absorbance of donors at 345 nm, c is the concentration of DNA junction, and l is the optical path length. Where I_{DA} is the emission intensity of donors in DNA junction with acceptor, and I_{D} is the emission intensity of donors in DNA junction without acceptor.

2-4-2 Absorption spectrum of DNA junction

Absorption spectrum measurements were performed to obtain the A_{D} needed to calculate the absorption coefficients of donors. The results are shown in Fig. 2-2.

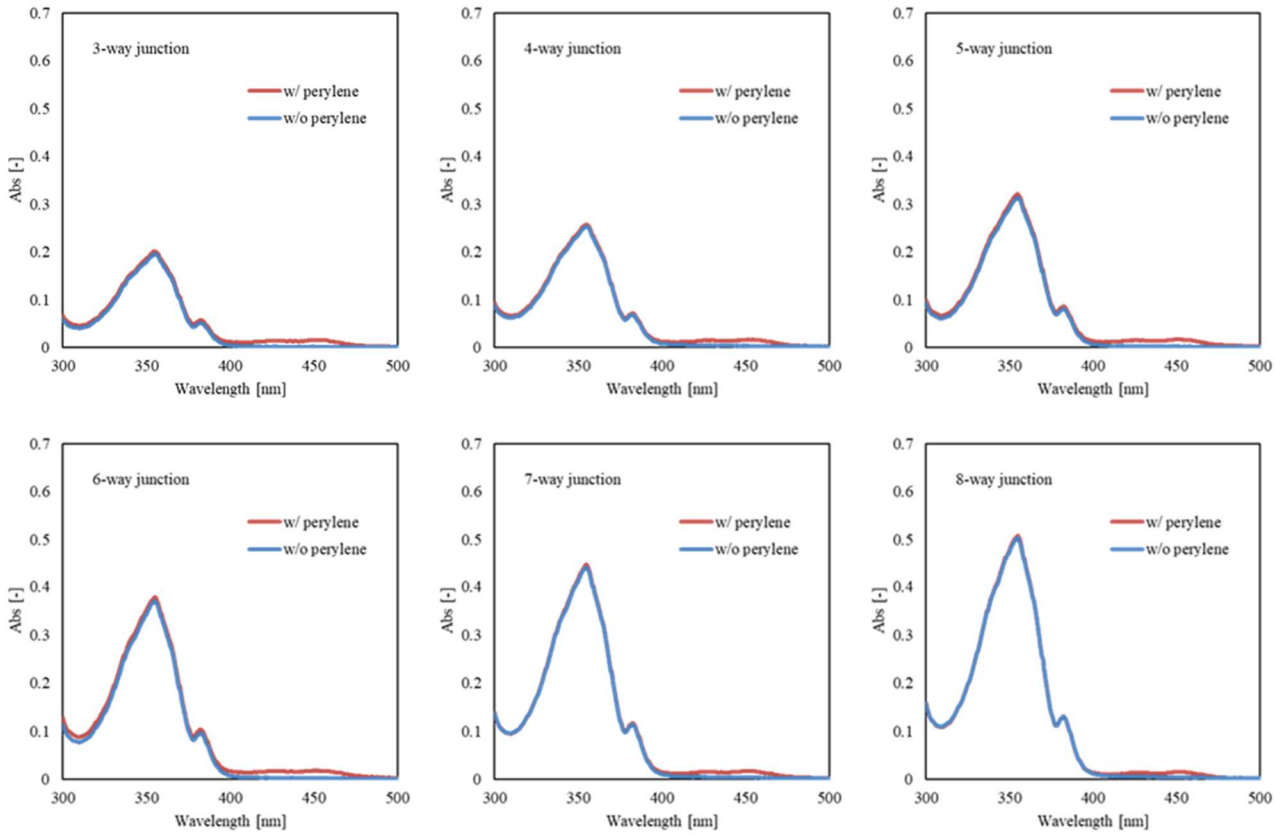

Figure 2-2. Absorption spectra of DNA junction.

Conditions

[DNA] = 0.5 μM, [$MgCl_2$] = 10 mM, pH = 7.0 (10 mM HEPES buffer), 20 ℃

The introduction of perylene caused a new absorption peak around 450 nm, which is the absorption wavelength of perylene. The absorbance of the donor was proportional to the number of arms of the DNA junction.

2-4-3 Emission spectrum of DNA junctions

Steady-state fluorescence spectral measurements were performed to obtain the I_D and I_{DA} needed to calculate FRET efficiencies. The results are shown in Fig. 2-3.

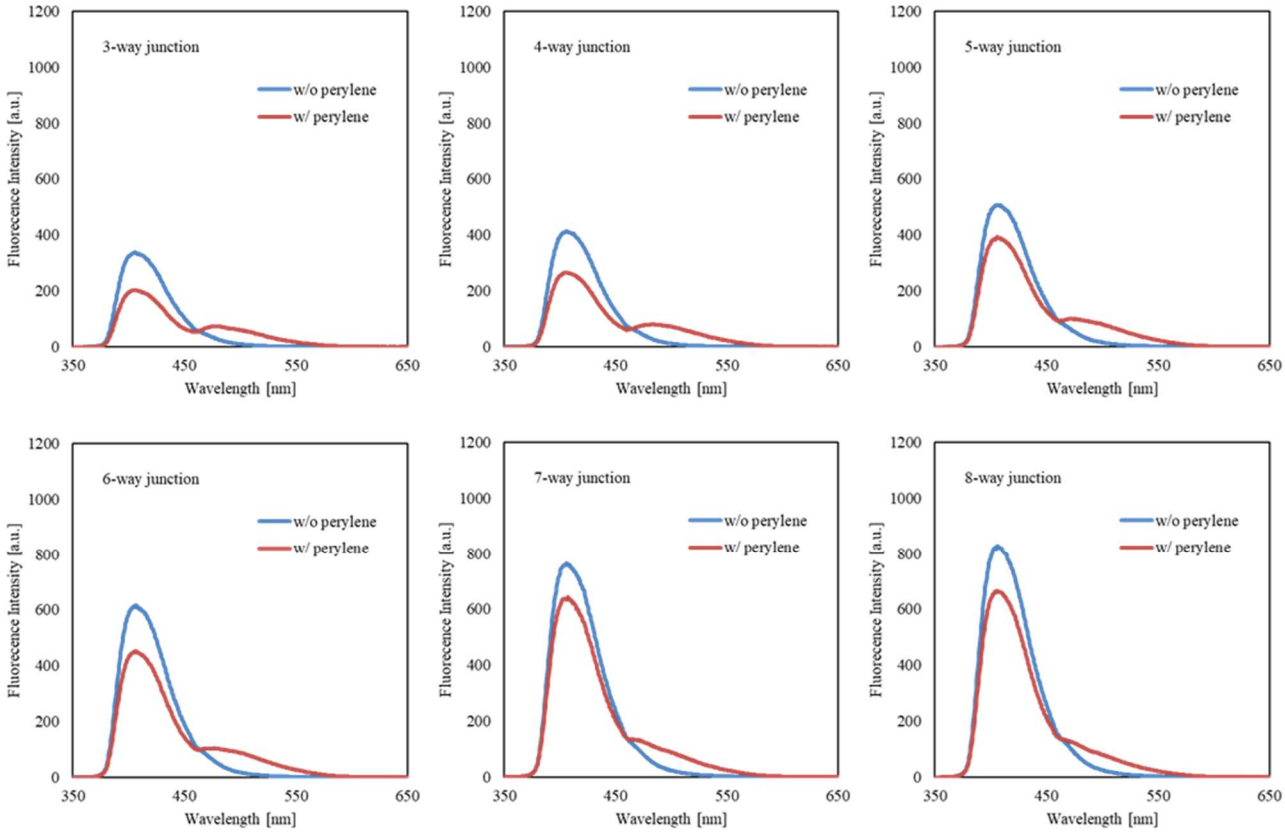

Figure 2-3 Steady-state fluorescence spectra of DNA junction.

Conditions

[DNA] = 0.5 μM, [$MgCl_2$] = 10 mM, pH = 7.0 (10 mM HEPES buffer), 20 ℃, Excitation = 345 nm

With the introduction of perylene, a decrease in the fluorescence intensity of pyrene and the appearance of perylene fluorescence were observed. This confirms that FRET occurs between pyrene and perylene as designed.

2-4-4 Calculation of effective absorption coefficients

ε_Ds of each DNA junction were calculated from absorption spectra. Φ_Ts of each DNA junction were calculated from the steady-state fluorescence spectra. ε_{eff}s were calculated from the ε_Ds and Φ_Ts. Results are shown in Table 2-1 and Fig. 2-4.

Table 2-1. ε_Ds, Φ_Ts and ε_{eff}s of DNA junction.

		Duplex	3-way junction	4-way junction	5-way junction	6-way junction	7-way junction	8-way junction
ε_D	$\times 10^5 M^{-1}cm^{-1}$	2.27	3.38	4.37	5.38	6.37	7.55	8.68
Φ_T		0.42	0.40	0.36	0.22	0.27	0.16	0.20
ε_{eff}	$\times 10^5 M^{-1}cm^{-1}$	0.96	1.36	1.57	1.20	1.69	1.19	1.70

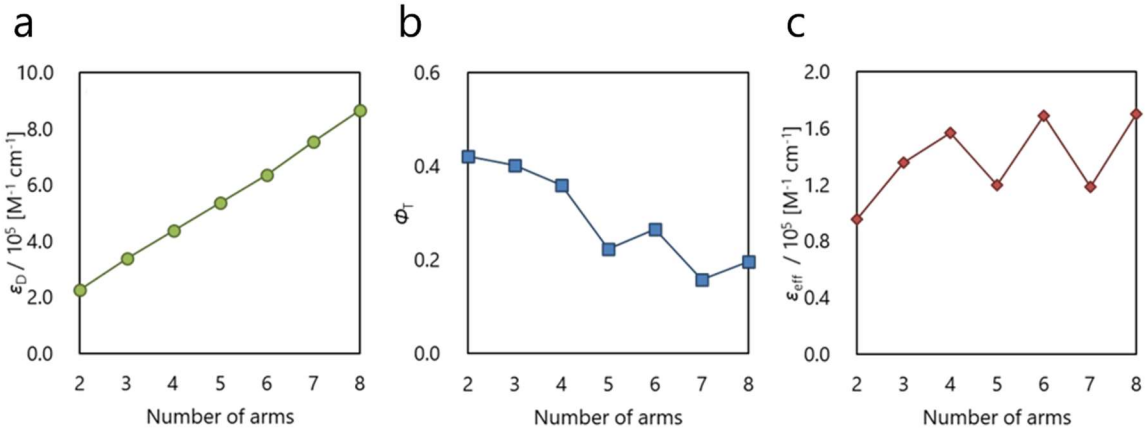

Figure 2-4. (a) ε_Ds, (b) Φ_Ts and (c) ε_{eff}s of DNA junction.

ε_Ds were proportional to the number of arms of the DNA junction. This result is expected because the number of pyrene introduced into the DNA junction is proportional to the number of arms. Φ_Ts decreased as the number of arms increased. Very interestingly, Φ_Ts showed odd-even effect: Φ_T is higher when the number of arms is even than when the number is odd. Since Φ_Ts showed odd-even effect, ε_{eff}s also showed odd-even effect. As a result, ε_{eff}s were highest at the 6-way and 8-way junction. Their ε_{eff}s were about 8.5 times higher than the maximum absorption coefficient of perylene alone, 2.0×10^4 M^{-1} cm^{-1}. Based on the above, we have succeeded in developing a highly efficient light-harvesting antenna by accumulating multiple fluorophores into DNA junction.

2-4-5 Confirmation of DNA junction formation

Native PAGE was performed to confirm the formation of DNA junction. The results are shown in Fig. 2-5. The calculated yields of each DNA junction calculated from band intensity ratios are shown in Fig. 2-6 and Table 2-2.

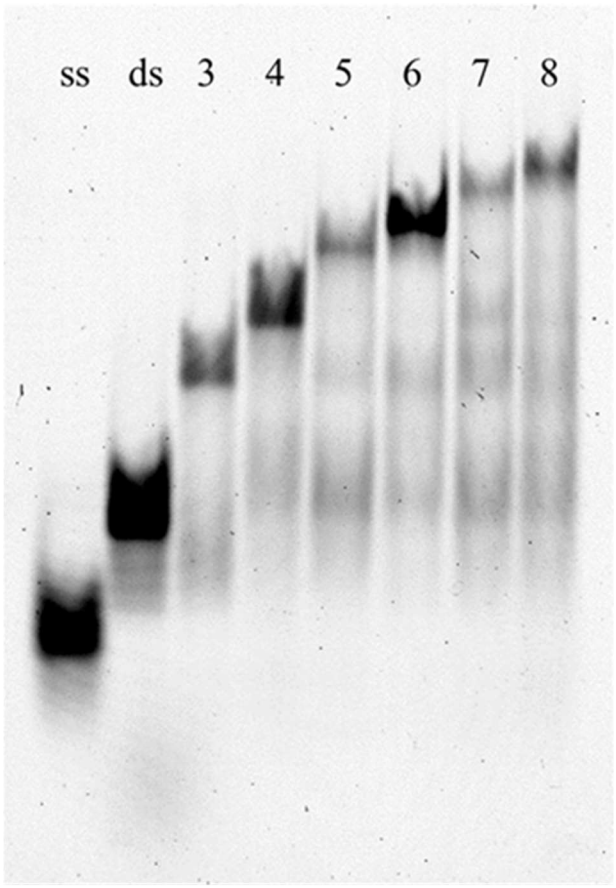

Figure 2-5. Native PAGE image of DNA junctions.

Conditions

[DNA] = 0.5 μM, [$MgCl_2$] = 10 mM, pH = 7.0 (10 mM HEPES buffer), 0 ℃

5% nondenaturing polyacrylamide gel (with glycerol), ×1 TB buffer ([$MgCl_2$] = 10 mM)

Table 2-2. Yields and Φ_Ts of DNA junction.

	Duplex	3-way junction	4-way junction	5-way junction	6-way junction	7-way junction	8-way junction
Yield	0.86	0.53	0.67	0.37	0.62	0.20	0.29
Φ_T	0.42	0.40	0.36	0.22	0.27	0.16	0.20

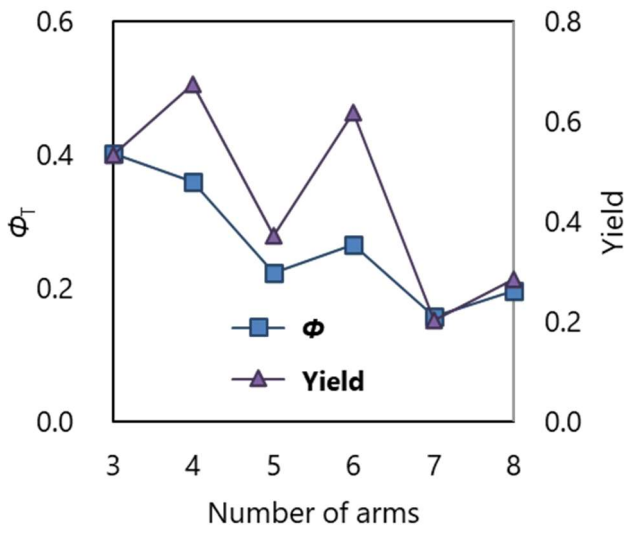

Figure 2-6. Yields of DNA junction.

The bands of each DNA junction appeared above the single strand and duplex. This indicates that all of the DNA junctions form a multimer as designed. The bands of DNA junction with even arms were denser than those of DNA junction with odd arms. In contrast, the bands of those that did not form the desired DNA junction at the bottom were thinner when the number of arms was even than when the number of arms was odd. As a result, the yields of DNA junctions showed odd-even effect as Φ_Ts. The yields decreased as the number of arms increased. These results suggest that the decrease in Φ_T is due to a decrease in the yield of DNA junction.

2-4-6 Fluorescence lifetime of donors

The results of Native PAGE suggested that the FRET efficiency of DNA junction is strongly affected by the yield of DNA junction. Therefore, fluorescence lifetime measurements were performed to calculate the FRET efficiency of only those that formed the desired DNA junction. The results are shown in Fig. 2-7.

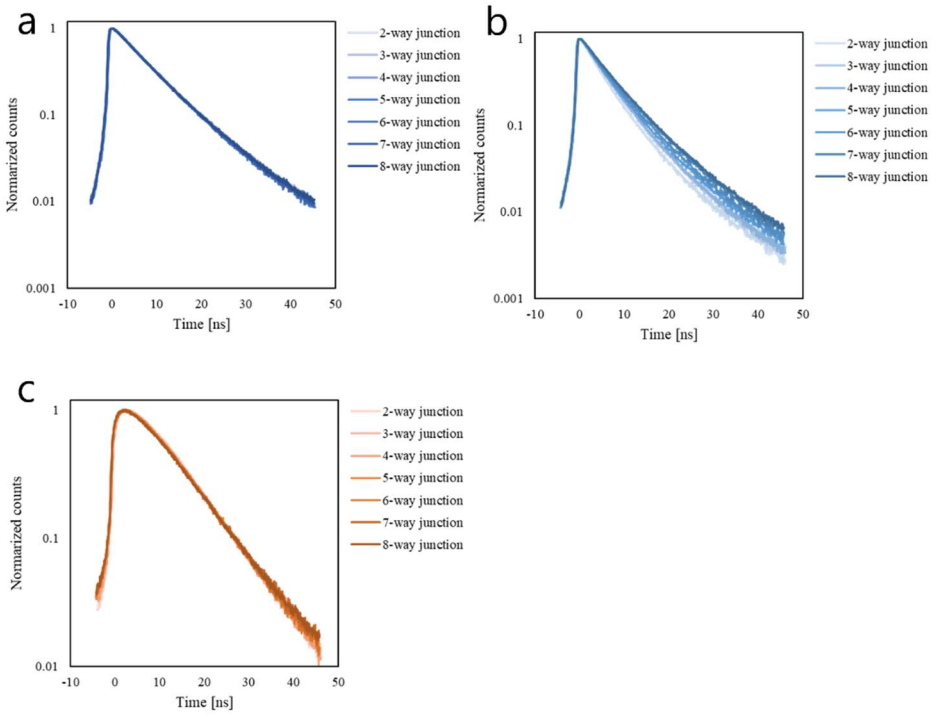

Figure 2-7. Fluorescence decay curve of pyrene in DNA junction.

Conditions

total [DNA] = 25 μM, [$MgCl_2$] = 10 mM, pH = 7.0 (10 mM HEPES buffer), r.t.

Excitation wavelength = 355 nm, Emission wavelength = 400 to 430 nm

The introduction of perylene caused the fluorescence of pyrene to decay faster, confirming that FRET was occurring between pyrene and perylene as designed.

The time variation of fluorescence intensity F_D when a fluorescent dye is excited by pulsed light is expressed by the following equation.

$$F_D = \exp(-kt)$$
$$= \exp(-t/\tau)$$

Where k is the energy transfer rate constant, and τ is the fluorescence lifetime.

The calculated fluorescence lifetimes of donors are shown in Table 2-3.

Table 2-3. τs and ks of DNA junction.

			Duplex	3-way junction	4-way junction	5-way junction	6-way junction	7-way junction	8-way junction
w/o acceptor	τ_D	[ns]	7.50	7.56	7.40	7.38	7.51	7.49	7.39
w/ acceptor	τ_{DA1}	[ns]	3.90	4.23	4.08	4.26	4.82	4.85	5.25
	α_{DA1}		0.79	0.81	0.74	0.68	0.76	0.70	0.79
	τ_{DA2}	[ns]	8.70	9.75	8.92	8.84	10.14	10.05	11.84
	α_{DA2}		0.21	0.19	0.26	0.32	0.24	0.30	0.21
	k	[ns^{-1}]	0.26	0.24	0.25	0.23	0.24	0.21	0.19

The fluorescence lifetime of the donor without acceptor can be fitted with one component (τ_D), while that of the donor with acceptor can be fitted with two components (τ_{DA1} and τ_{DA2}). The longer fluorescence lifetime components (τ_{DA2}) of the donor with acceptor were similar to these of the donor without acceptor, suggesting the presence of a donor that is not involved in energy transfer to the acceptor. The shorter fluorescence lifetime components (τ_{DA1}) are considered to be the components that energy transferred from the donors to the acceptor. The ratio of shorter fluorescence lifetime components (α_{DA1}) was higher when the number of arms was even than when the number was odd. This suggests that there is the odd-even effect in the yield of DNA junction .

The FRET efficiency of the desired DNA junction (Φ_T') is calculated by the following equation.

$$\Phi_T' = 1 - \tau_{DA}/\tau_D$$

Where τ_{DA} is the fluorescence lifetime of donors with acceptor, and τ_D is the fluorescence lifetime of donors without acceptor.

Φ_T' and the effective absorption coefficients of desired DNA junction (ε_{eff}'s) calculated from the fluorescence decay curve are shown in Table 2-4 and Fig. 2-8.

Table 2-4. Φ_T's and ε_{eff}'s of DNA junction.

	Duplex	3-way junction	4-way junction	5-way junction	6-way junction	7-way junction	8-way junction
Φ_T,	0.48	0.44	0.45	0.42	0.36	0.35	0.29
ε_{eff}' $\times 10^5 M^{-1}cm^{-1}$	1.09	1.49	1.96	2.28	2.28	2.66	2.51

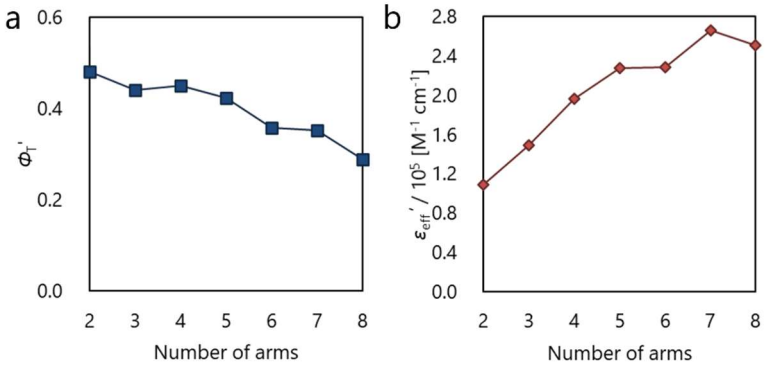

Figure 2-8. Φ_T's and ε_{eff}'s of DNA junction.

Unlike Φ_Ts, Φ_T's did not show odd-even effect. This indicates that the number of arms of the DNA junction does not affect the energy transfer. ε_{eff}'s reached a maximum of 2.7×10^5 M^{-1} cm^{-1} at the 7-way junction. Its ε_{eff}' increased about 13 times compared to the maximum absorption coefficient of perylene alone, 2.0×10^4 M^{-1} cm^{-1}.

2-4-7 Simulation of energy transfer

We attempted to simulate the energy transfer in the light-harvesting antenna based on the parameters obtained from the analysis of hetero FRET of pyrene-perylene and homo FRET of pyrene-pyrene, which have been performed in our laboratory in the past. The energy transfer rate constants required for the simulation are obtained from the distance and orientation between each dye. Therefore, molecular modeling of the duplex was performed. The results are shown in Fig. 2-9 Table 2-5 shows the results of measuring the distance and orientation between each dye and calculating each energy transfer rate constant.

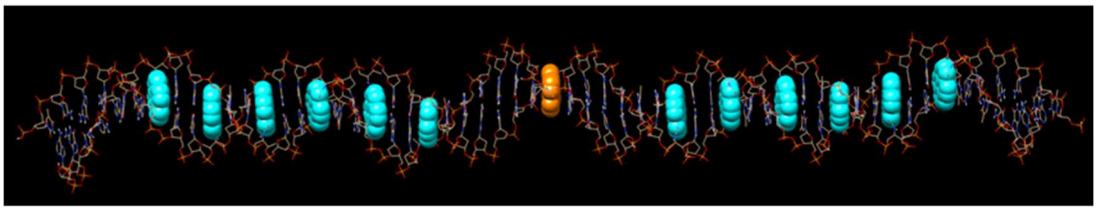

Figure 2-9. Molecular modeling of DNA duplexes with accumulated fluorophores. Pyrens are shown in blue and perylene is shown in orange.

Table 2-5. Energy transfer rate between fluorophores.

		r [Å]	θ [rad]	R [Å]	Φ_T	k [s^{-1}]
E	P1	23.2	59.2	34.92	0.92	1.17×10^{9}
E	P2	32.7	-90.3	7.22	0.00	1.16×10^{4}
E	P3	42.7	-112.7	31.85	0.15	1.72×10^{7}
E	P4	52.5	97.9	22.56	0.01	6.32×10^{5}
E	P5	62.2	74.1	28.37	0.01	9.03×10^{5}
E	P6	71.8	-85.7	18.50	0.00	2.93×10^{4}
P1	P2	9.8	-150.3	23.32	0.99	1.78×10^{10}
P1	P3	20.2	-173.5	24.40	0.76	3.15×10^{8}
P1	P4	29.7	37.1	22.68	0.17	2.00×10^{7}
P1	P5	39.3	13.9	24.21	0.05	5.44×10^{6}
P1	P6	49.2	-146.0	22.97	0.01	1.04×10^{6}
P2	P3	10.6	-21.5	23.87	0.99	1.28×10^{10}
P2	P4	20.0	-172.4	24.38	0.77	3.32×10^{8}
P2	P5	29.5	164.3	24.14	0.23	2.98×10^{7}
P2	P6	39.3	4.3	24.43	0.05	5.74×10^{6}
P3	P4	9.8	-149.0	23.23	0.99	1.73×10^{10}
P3	P5	20.0	-172.3	24.38	0.76	3.25×10^{8}
P3	P6	29.6	27.3	23.50	0.20	2.50×10^{7}
P4	P5	10.5	-21.3	23.88	0.99	1.39×10^{10}
P4	P6	20.1	176.9	24.44	0.77	3.26×10^{8}
P5	P6	10.1	-159.2	23.90	0.99	1.80×10^{10}

The calculated rate constants suggest that the energy transfer between pyrene and perylene occurs only from the first pyrene, and the energy transfer between pyrene and pyrene from one and two pyrene apart.

The time derivatives of the fraction Pn of the excited state of the n-th donor counting from the nearest acceptor is expressed as following equations.

$$dP_1/dt = -(k_{\mathrm{D}} + k_{\mathrm{D1A}} + k_{12} + k_{13} + k_{14} + k_{15} + k_{16})P_1 + k_{21}P_2 + k_{31}P_3 + k_{41}P_4 + k_{51}P_5 + k_{61}P_6$$

$$dP_2/dt = -(k_{\mathrm{D}} + k_{\mathrm{D2A}} + k_{21} + k_{23} + k_{24} + k_{25} + k_{26})P_2 + k_{12}P_1 + k_{32}P_3 + k_{42}P_4 + k_{52}P_5 + k_{62}P_6$$

$$dP_3/dt = -(k_{\mathrm{D}} + k_{\mathrm{D3A}} + k_{31} + k_{32} + k_{34} + k_{35} + k_{36})P_3 + k_{13}P_1 + k_{23}P_2 + k_{43}P_4 + k_{53}P_5 + k_{63}P_6$$

$$dP_4/dt = -(k_{\mathrm{D}} + k_{\mathrm{D4A}} + k_{41} + k_{42} + k_{43} + k_{45} + k_{46})P_4 + k_{14}P_1 + k_{24}P_2 + k_{34}P_3 + k_{54}P_5 + k_{64}P_6$$

$$dP_5/dt = -(k_{\mathrm{D}} + k_{\mathrm{D5A}} + k_{51} + k_{52} + k_{53} + k_{54} + k_{56})P_5 + k_{15}P_1 + k_{25}P_2 + k_{35}P_3 + k_{45}P_4 + k_{65}P_6$$

$$dP_6/dt = -(k_{\mathrm{D}} + k_{\mathrm{D6A}} + k_{61} + k_{62} + k_{63} + k_{64} + k_{65})P_6 + k_{16}P_1 + k_{26}P_2 + k_{36}P_3 + k_{46}P_4 + k_{56}P_5$$

Where k_{D} is the fluorescence emission rate constant of donor, k_{DnA} is the energy transfer constant from n-th donor to the acceptor, and k_{nm} is the energy transfer constant from n-th donor to m-th donor.

Simulation of time variation of fluorescence intensity was performed by solving differential equations with rate constants calculated from molecular modeling. The results are shown in Fig.2-10.

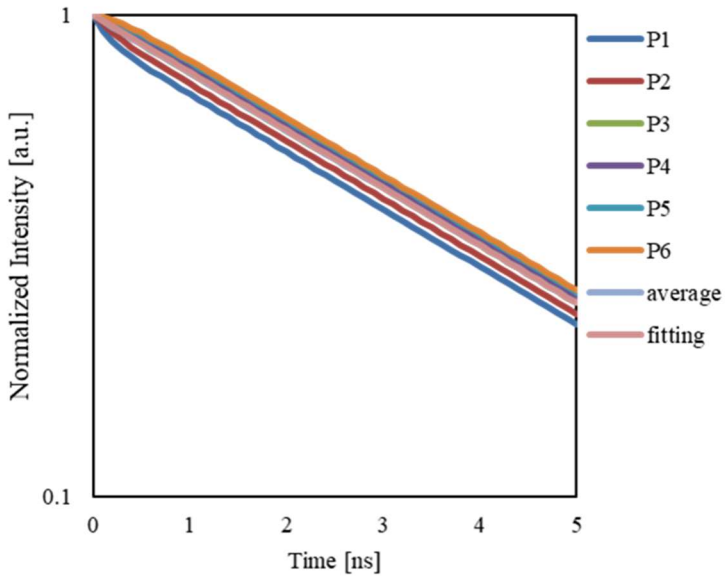

Figure 2-10. Simulation of fluorescence decay curve.

The fluorescence lifetime and the energy transfer constant calculated by fitting from the simulated time variation of fluorescence intensity are shown in Table 2-6.

Table 2-6. Fluorescence lifetimes and energy transfer constants.

		fluorescence lifetime	simulation
τ_D	[ns]	7.50	10.00
τ_{DA1}	[ns]	3.90	2.62
α_{DA1}		0.79	1.00
τ_{DA2}	[ns]	8.70	
α_{DA2}		0.21	
k	[ns^{-1}]	0.26	0.38

The fact that the fluorescence lifetime could be fitted with a single component suggests that the entire pyrene behaves as a single fluorophore and transfers energy to perylene due to the fast energy transfer between pyrene. The calculated energy transfer rate constant between pyrene and perylene was similar to that calculated from the single-life component of the fluorescence lifetime. This suggests that the energy transfer is occurring as designed.

2-5 Conclusion

In this study, we developed highly efficient light harvesting antennae by accumulating multiple pyrene as donor and a perylene as acceptor into DNA junction. The fluorophores were densely accumulated by using DNA junction. Fluorophores introduced via D-threoninol are fixed in

orientation, which enables strict dye alignment and highly efficient FRET can be expected. DNA junction with a large number of arms can accumulate a large number of donors and thus absorb a large amount of light. FRET efficiency was inversely proportional to the number of arms and showed odd-even: FRET efficiency is higher when the number of arms is even than when the number is odd. This is due to differences in the yields of DNA junction, and it is clear that there is the odd-even effect in the yields of DNA junction. The antenna effects were highest at the 6-way and 8-way junctions, where the antenna effect was about 8.5 times. The FRET efficiency of the desired DNA junction, calculated from the fluorescence lifetime of the donor, did not show the odd-even effect. The simulations yielded energy transfer rate constants comparable to the experimental values. This system can be used for high brightness labeling agents and artificial photosynthesis systems.

2-6 Experimental section

Materials

All conventional phosphoramidite monomers, CPG columns, reagents for DNA synthesis, and Poly-Pak II cartridges were purchased from Glen Research. Other reagents for the synthesis of phosphoramidite monomers were purchased from Tokyo Chemical Industry, Wako, and Aldrich. Native oligodeoxyribonucleotides (ODNs) were purchased from Integrated DNA Technologies. ODNs tethering pyrene and perylene were synthesized on an automated DNA synthesizer (H-8-SE, Gene World) ODNs were purified by gel electrophoresis and reversed-phase HPLC and characterized by MALDI-TOF MS (Autoflex maX, Bruker Daltonics) and HPLC.

Fluorescence measurements

Fluorescence spectra were measured on JASCO models FP-6500. The excitation wavelength was 345 nm. Band widths were 3 nm for excitation and emission. Before measurements, sample solutions containing DNA duplex or DNA junction were heated at 80 oC, then slowly cooled down to 20 ˚C at a rate of 1 ˚C min-1. Emission spectra shown in this paper were measured at 20 ºC unless otherwise noted. Sample solutions contained 10 mM MgCl2, 10 mM HEPES buffer (pH 7.0), 0.1 μM each oligonucleotides, unless otherwise noted.

Fluorescence lifetime measurements

Fluorescence lifetime measurements were performed by a photon-counting mode of a streak scope (Hamamatsu photonics, C7700), which has a spectrograph (Hamamatsu photonics, C11119-1) and a CCD camera (Hamamatsu photonics, C10600). The thirdharmonics of Nd:YAG laser (EKSPLA 2210A, fwhm 20 ps, 1 kHz) was used as an excitation source. A pre-trigger from the Nd:YAG laser system was delayed by a pulsed generator (DG535, Stanford research systems)

to use the synchronized operation for the streak scope with Nd:YAG laser. Decay curves of donor emission were obtained from the integration of the photon counts in the spectral region from 400 to 430 nm in the streak images. The fluorescence decay curve were analysed using the equipped software of the streak scope (HPDTA9.1, Hamamatsu photonics). The decay curves were fitted with the bi-exponential function $\alpha_1\exp(-t/\tau_1) + \alpha_2\exp(-t/\tau_2)$.

Absorption measurements

Absorption spectra were measured on a JASCO model V-530. Sample solution contained 0.5 μM each strand, 10 mM $MgCl_2$, 10 mM HEPES buffer (pH 7.0). Before measurements, sample solutions containing DNA duplex or DNA junction were heated at 80 ºC, then slowly cooled down to 20 ºC at a rate of 1 ºC min^{-1}. Absorption spectra shown in this paper were measured at 20 ºC unless otherwise noted.

Polyacrylamide gel electrophoresis

The samples were cooled from 80˚C to 0˚C at a rate of 1 ºC min^{-1} and then loaded onto a 5% polyacrylamide gel with 5% glycerol (1×TB buffer containing 10 mM $MgCl_2$). The temperature of the gel was kept constant during electrophoresis by using a water bath holder in which iced water was circulated. After gel electrophoresis, the gel was analyzed with an FLA-3000 bio-imaging analyzer (Fujifilm).

2-7 References

1. Lüer, L.; Moulisová, V.; Henry, S.; Polli, D.; Brotosudarmo, T. H. P.; Hoseinkhani, S.; Brida, D.; Lanzani, G.; Cerullo, G.; Cogdell, R. J., Tracking energy transfer between light harvesting complex 2 and 1 in photosynthetic membranes grown under high and low illumination. *Proceedings of the National Academy of Sciences* **2012,** *109* (5), 1473-1478.
2. Gunderson, V. L.; Smeigh, A. L.; Kim, C. H.; Co, D. T.; Wasielewski, M. R., Electron Transfer within Self-Assembling Cyclic Tetramers Using Chlorophyll-Based Donor–Acceptor Building Blocks. *Journal of the American Chemical Society* **2012,** *134* (9), 4363-4372.
3. Yang, J.; Yoon, M.-C.; Yoo, H.; Kim, P.; Kim, D., Excitation energy transfer in multiporphyrin arrays with cyclic architectures: towards artificial light-harvesting antenna complexes. *Chemical Society Reviews* **2012,** *41* (14), 4808-4826.
4. Benvin, A. L.; Creeger, Y.; Fisher, G. W.; Ballou, B.; Waggoner, A. S.; Armitage, B. A., Fluorescent DNA Nanotags: Supramolecular Fluorescent Labels Based on Intercalating Dye Arrays Assembled on Nanostructured DNA Templates. *Journal of the American Chemical Society* **2007,** *129* (7), 2025-2034.
5. Probst, M.; Langenegger, S. M.; Häner, R., A modular LHC built on the DNA three-

way junction. *Chemical Communications* **2014,** *50* (2), 159-161.

6. Buckhout-White, S.; Spillmann, C. M.; Algar, W. R.; Khachatrian, A.; Melinger, J. S.; Goldman, E. R.; Ancona, M. G.; Medintz, I. L., Assembling programmable FRET-based photonic networks using designer DNA scaffolds. *Nature Communications* **2014,** *5* (1), 5615.

7. Kato, T.; Kashida, H.; Kishida, H.; Yada, H.; Okamoto, H.; Asanuma, H., Development of a Robust Model System of FRET using Base Surrogates Tethering Fluorophores for Strict Control of Their Position and Orientation within DNA Duplex. *Journal of the American Chemical Society* **2013,** *135* (2), 741-750.

8. Kawai, H.; Doi, T.; Ito, Y.; Kameyama, T.; Torimoto, T.; Kashida, H.; Asanuma, H., Perylene-Cy3 FRET System to Analyze Photoactive DNA Structures. *Chemistry – A European Journal* **2021,** *27* (50), 12845-12850.

9. Fujii, T.; Kashida, H.; Asanuma, H., Analysis of Coherent Heteroclustering of Different Dyes by Use of Threoninol Nucleotides for Comparison with the Molecular Exciton Theory. *Chemistry – A European Journal* **2009,** *15* (39), 10092-10102.

2-8 Appendixes

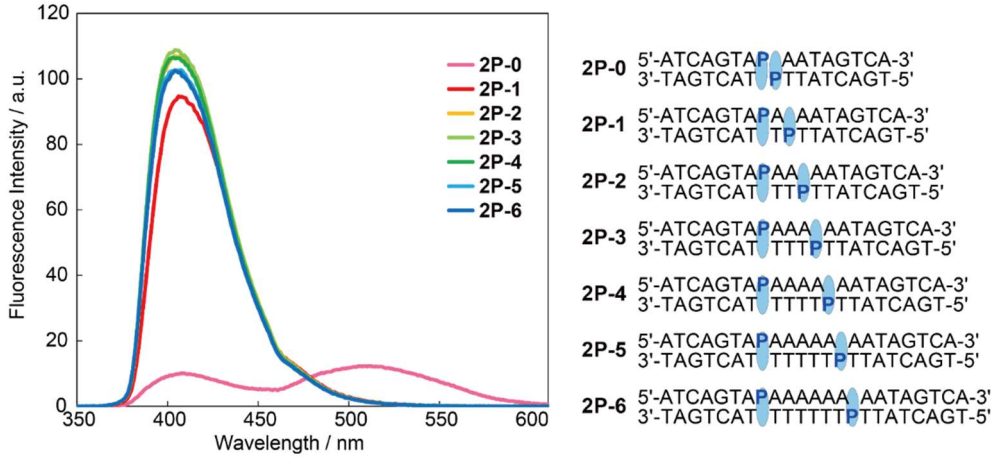

Figure S2-1. Effect of the number of base pairs between two pyrene residues on the emission of pyrene. Sequences used for the evaluation are listed at the right. Conditions: [DNA] = 1.0 μM, 100 mM NaCl, 10 mM phosphate buffer (pH 7.0).

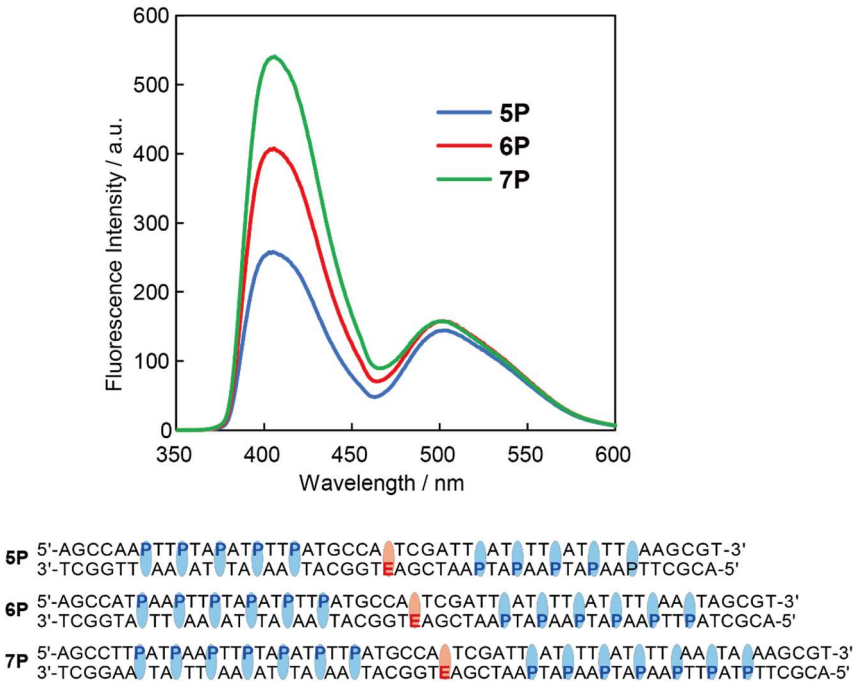

Figure S2-2. Effects of the number of pyrene residues on the emission spectra. Sequences are shown below. Sequences used for the evaluation are listed at the right. Conditions: [DNA] = 1.0 μM, 100 mM NaCl, 10 mM phosphate buffer (pH 7.0).

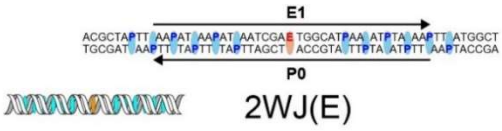

2WJ(E)

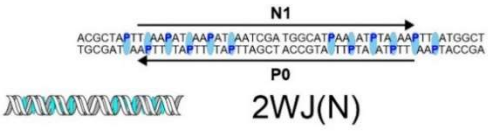

2WJ(N)

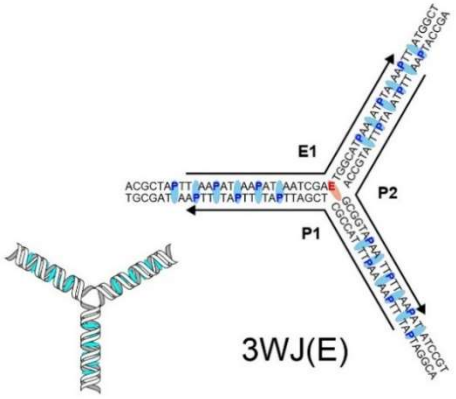

3WJ(E)

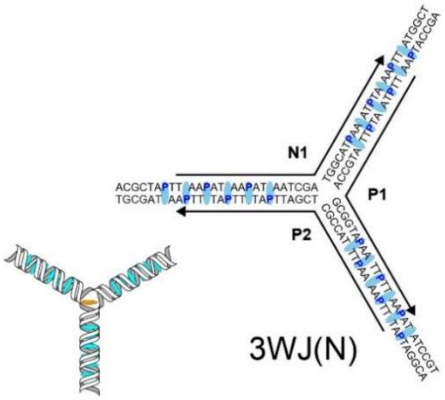

3WJ(N)

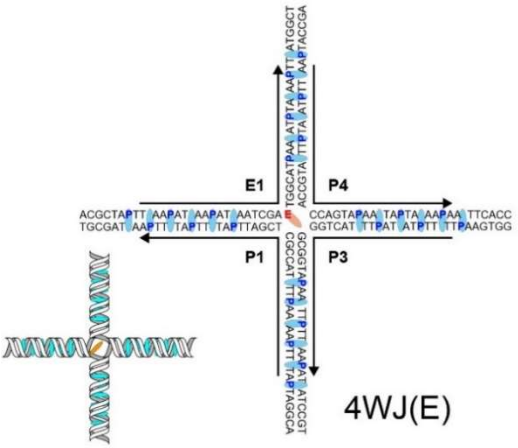

4WJ(E)

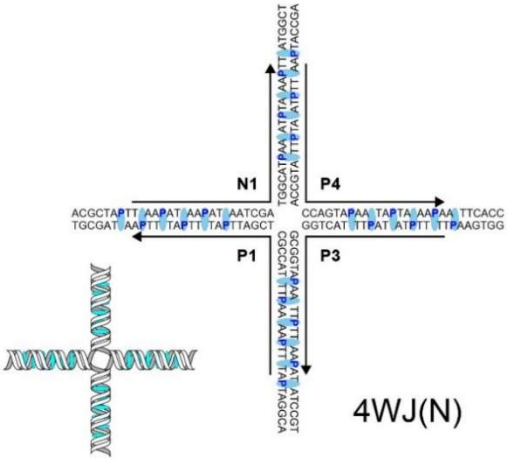

4WJ(N)

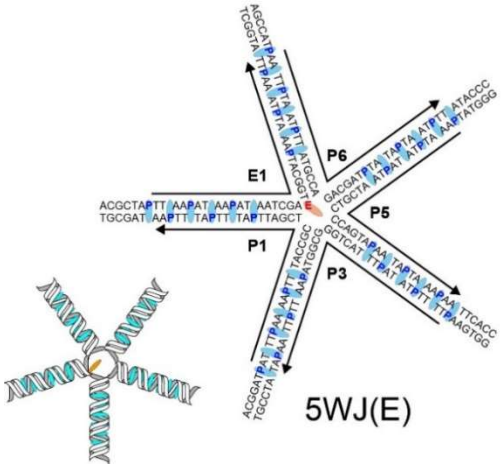

5WJ(E)

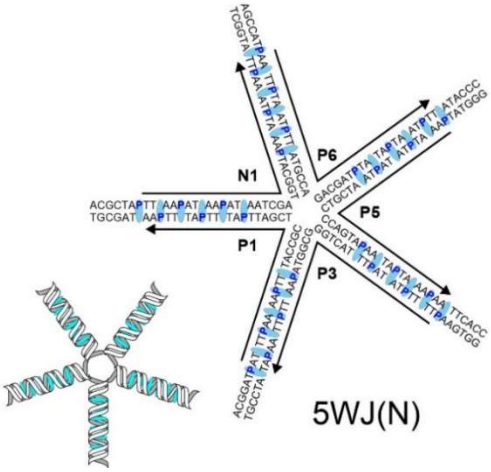

5WJ(N)

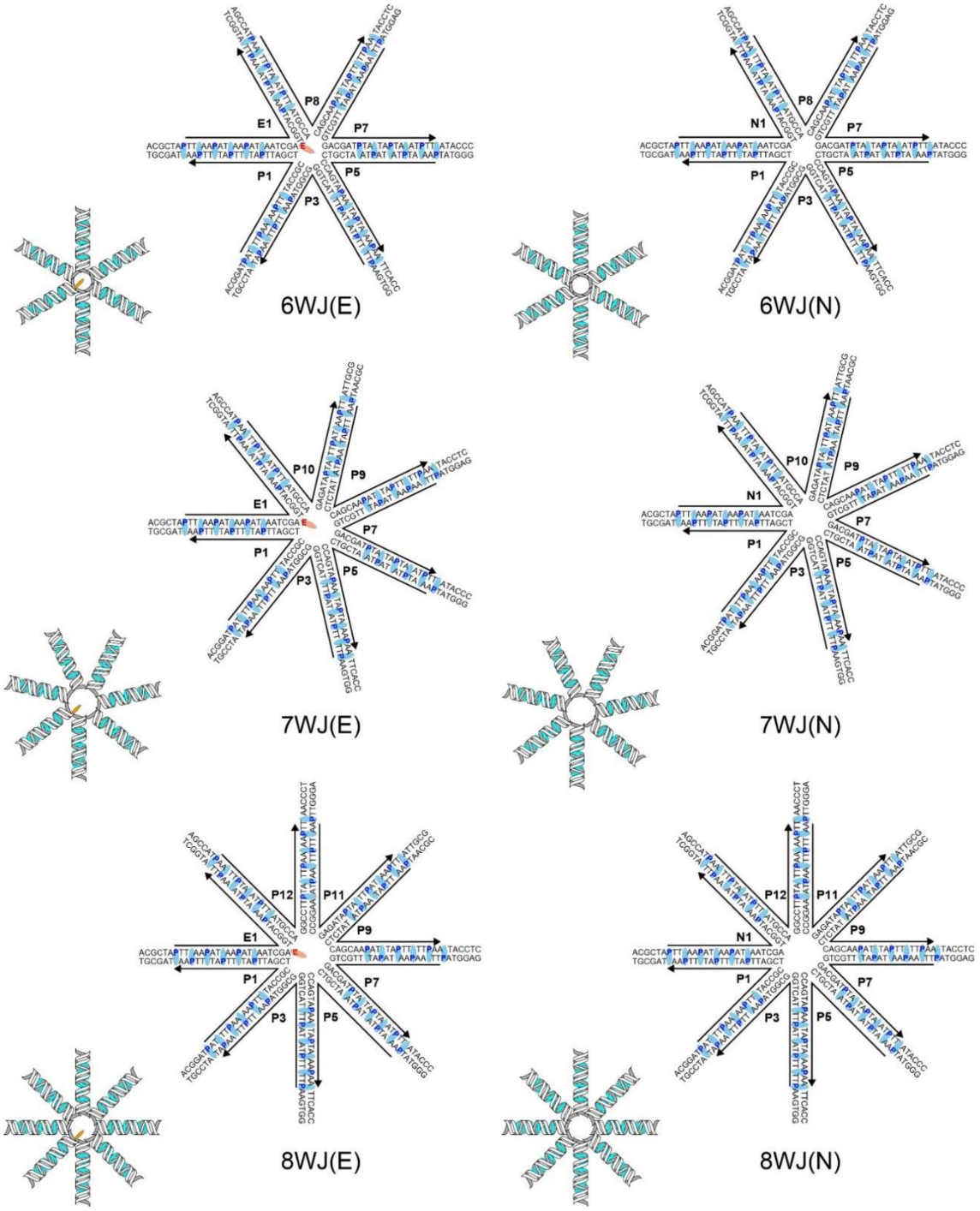

Figure S2-3. Sequences of oligonucleotides used to prepare junctions.

Table S2-1 DNA sequence.

Name	Sequence (5’→3’)
E	ACGCTAPTTAAPATAAPATAATCGAETGGCATPAAATPTAAAPTTATGGCT
N	ACGCTAPTTAAPATAAPATAATCGATGGCATPAAATPTAAAPTTATGGCT
P0	AGCCATPAATTPTAATPTTATGCCATCGATTPATTTPATTTPAATAGCGT
P1	ACGGATPATTTPAAAAPTTTACCGCTCGATTPATTTPATTTPAATAGCGT
P2	AGCCATPAATTPTAATPTTATGCCAGCGGTAPAATTPTTAAPATATCCGT
P3	GGTGAAPTTTTPTATAPTTTACTGGGCGGTAPAATTPTTAAPATATCCGT
P4	AGCCATPAATTPTAATPTTATGCCACCAGTAPAATAPTAAAPAATTCACC
P5	GGGTATPAAATPTATAPTAATCGTCCCAGTAPAATAPTAAAPAATTCACC
P6	AGCCATPAATTPTAATPTTATGCCAGACGATPTATAPTAATPTTATACCC
P7	GAGGTAPTTAAPAATAPATTTGCTGGACGATPTATAPTAATPTTATACCC
P8	AGCCATPAATTPTAATPTTATGCCACAGCAAPATTAPTTTTPAATACCTC
P9	CGCAATPAATTPATAAPTATATCTCCAGCAAPATTAPTTTTPAATACCTC
P10	AGCCATPAATTPTAATPTTATGCCAGAGATAPTATTPATAAPTTATTGCG
P11	AGGGTTPAATTPTTAAPTAAAGGCCGAGATAPTATTPATAAPTTATTGCG
P12	AGCCATPAATTPTAATPTTATGCCAGGCCTTPTATTPAAAAPTTAACCCT

P: pyrene, E: perylene

Capter 3 Investigation of energy transfer from dyes to metal complexes (Förster energy transfer from metal complex to dye)

3-1 Abstract

We developed a novel FRET system dependent only on distance. Pyrene as FRET donor and $Ru(bpy)_3$ as acceptor were introduced via D-threoninol at the DNA junction. The symmetry of $Ru(bpy)_3$ cancels the orientation dependence of FRET. The motility of molecules introduced via D-threoninol is low. A novel bpy monomer was designed and synthesized to synthesize $Ru(bpy)_3$-DNA conjugate. $Ru(bpy)_3$-DNA conjugate was synthesized from the ligand exchange reaction of bpy-DNA conjugate. FRET from pyrene to $Ru(bpy)_3$ in DNA junctions was shown to cancel the orientation dependence and depend only on the distance. This system can be used for a nano-ruler or a simplification of complex energy transfer systems.

3-2 Introduction

Measurements of the size of biomolecules and the distances between biomolecules in vivo reveal molecular dynamics in vivo. X-ray crystallography [1 2] and cryo-electron microscopy [3-4] are often used to obtain structural information on biomolecules. The structures obtained from these methods provide a large amount of information and can predict accurate structures at the atomic level. However, it is impossible to observe the molecular dynamics in a living state or over time because the molecules must be completely immobilized for measurement.

Förster resonance energy transfer (FRET) is a phenomenon in which light energy is transferred between dyes and its efficiency depends on the distance and orientation between dyes [5]. Since dye orientation is difficult to control and dyes are assumed to be freely rotating, the FRET efficiency between molecules gives the distance between molecules. FRET probe can be used as a molecular ruler because the FRET efficiency between dyes gives the distance between molecules. FRET is observed by light irradiation, which allows us to observe the molecular structure and molecular dynamics in a living state. Furthermore, single-molecule FRET (smFRET) can be used to observe the dynamics of a single molecule. The FRET probe has been used to observe the dynamics of proteins [6 7], nucleic acids [8 9], and fluorescent biomolecules [10 11].

However, rotation of the dye and movement of the dye when using long linkers are inevitable, and the distance is not always accurately measured.

In this study, we developed a novel molecular ruler for precise measurement of dye distances. Pyrene as donor and tris(2,2'-bipyridine) ruthenium(II) ($Ru(bpy)_3$) as acceptor for FRET were introduced into the DNA junction via D-threoninol linker. Since $Ru(bpy)_3$ has three transition

dipole moments in spatially symmetric orientations [12], it is expected to cancel the orientation dependence of the FRET. Molecules introduced via the short D-threoninol linker have low motility, especially the smaller sized molecules, which are introduced between the base pairs of the DNA, thus fixing the orientation almost completely [13]. FRET that depends only on distance is expected.

3-3 Design

Pyrene was selected as the donor for energy transfer and tris(2,2'-bipyridine) ruthenium(II) ($Ru(bpy)_3$) as the acceptor. Since there is a large overlap between the emission spectrum of Pyrene and the absorption spectrum of $Ru(bpy)_3$ (Fig. S3-1), highly efficient energy transfer can be expected. Since $Ru(bpy)_3$ has transition dipole moments in spatially symmetric orientations, it is expected to cancel the orientation dependence of the FRET from pyrene. $Ru(bpy)_3$ was placed in the center of the 3-way DNA junction and pyrene was introduced at the duplex site. Furthermore, the base pairing between pyrene and $Ru(bpy)_3$ was varied from 0 bp to 19 bp and the fluorescence spectrum was measured. DNA junctions with perylene as the acceptor in the center were also prepared in the same way for comparison with the case where the acceptor was an organic dye, and the fluorescence spectra were measured to calculate the energy transfer efficiency. The energy transfer efficiency at each base pair distance was calculated from the percentage decrease in fluorescence intensity of the donor due to the introduction of the acceptor.

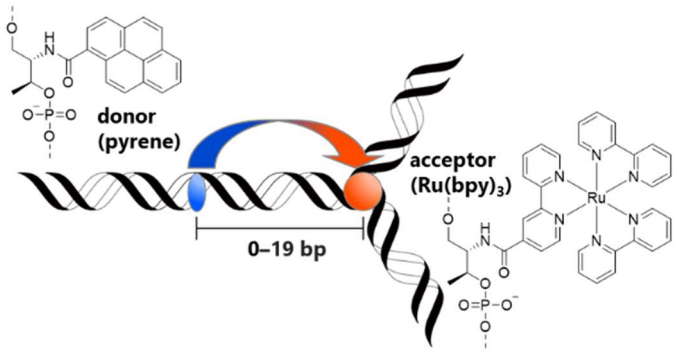

Figure3-1 Design of FRET system from pyrene to $Ru(bpy)_3$ in DNA 3-way junction.

3-4 Results and discussions

3-4-1 Synthesis and characterization of $Ru(bpy)_3$-DNA conjugates

The introduction of $Ru(bpy)_3$ into DNA was achieved by ligand exchange between bpy introduced into DNA and *cis*-dichlorobis(2,2'-bipyridine) ruthenium (II) ($Ru(bpy)_2Cl_2$). $Ru(bpy)_2Cl_2$ was synthesized based on a previous report[14]. DNA with a bpy in the center of poly-T as a test sequence was synthesized and subjected to a ligand exchange reaction with $Ru(bpy)_2Cl_2$ (Fig. 3-2). We synthesized 2-(pyridin-2-yl)pyridine-4-carboxylic acid based on a previous report

[15]. This carboxylic acid was combined with D-threoninol to synthesize phosphoramidite monomers and bpy-DNA conjugates were introduced into a DNA oligonucleotide during general solid-phase synthesis.

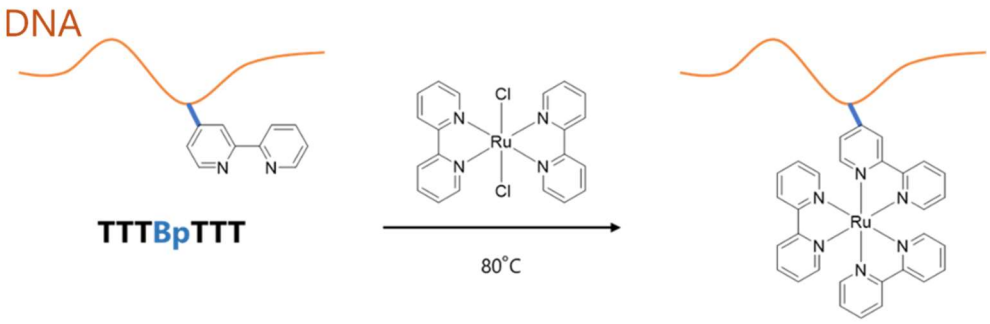

Figure 3-2. Synthesis of $Ru(bpy)_3$-DNA conjugate using ligand exchange reaction.

First, the sequence with bpy in poly-T (T6-Bp) was used as the test sequence. A ligand exchange reaction was performed under the conditions to synthesize $Ru(bpy)_3$ from general bpy and $Ru(bpy)_2Cl_2$.

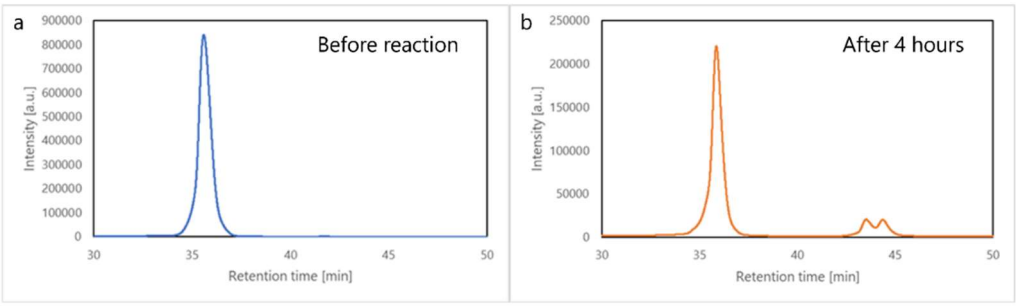

Figure 3-3. HPLC profiles (a) before and (a) after ligand exchange reaction under general conditions.

Conditions

[DNA-bpy] = 1 mM, $[Ru(bpy)_2Cl_2]$ = 2 mM

Buffer: H_2O:EtOH = 1:3, 200µl, 80 °C

Two new peaks appeared at 4 hours of reaction (Fig. 3-3b). The reaction did not progress any further even after extending the reaction time. After preparative analysis, mass spectrometry was performed and both were found to be consistent with the target Ru-DNA conjugates (T6-Ru) (calculated mass = 2525.47, first peak: observed mass = 2522.864, second peak: observed mass = 2523.472). From this we can say that the ligand exchange reaction is occurring correctly. However, the product peaks were small, a large amount of bpy-DNA conjugates remained, and the reaction efficiency was low.

The following two points were considered to be responsible for the low reaction efficiency.

- DNA has low solubility in ethanol.
- The negative charge of the phosphate groups of DNA inhibits the reaction.

Therefore, the organic solvent used was changed from ethanol to methanol. In addition, NaCl was added to increase the number of cations in the system, and the ligand exchange reaction was performed with a lower solvent ratio of methanol.

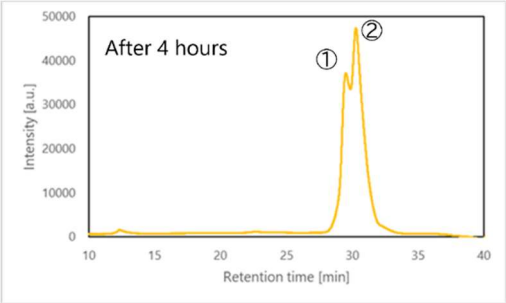

Figure 3-4. HPLC profiles before and after ligand exchange reaction under optimized conditions.

Conditions

[DNA-bpy] = 1 mM, [$Ru(bpy)_2Cl_2$] = 2 mM, [NaCl] = 50 mM

Buffer: H_2O:MeOH = 1:1, 200µl, 80 °C

The change in solvent greatly increased the efficiency of the reaction; after 4 hours, most of the bpy-DNA conjugates was consumed (Fig. 3-4). After preparative mass spectrometry, both were consistent with T6-Ru (first peak: observed mass = 2522.680, second peak: observed mass = 2522.648). This suggests that increasing the number of cations in the system improves the efficiency of the ligand exchange reaction.

To confirm that $Ru(bpy)_3$ was synthesized by the ligand exchange reaction performed in this study, we measured absorption spectrum and emission spectrum of T6-Ru.

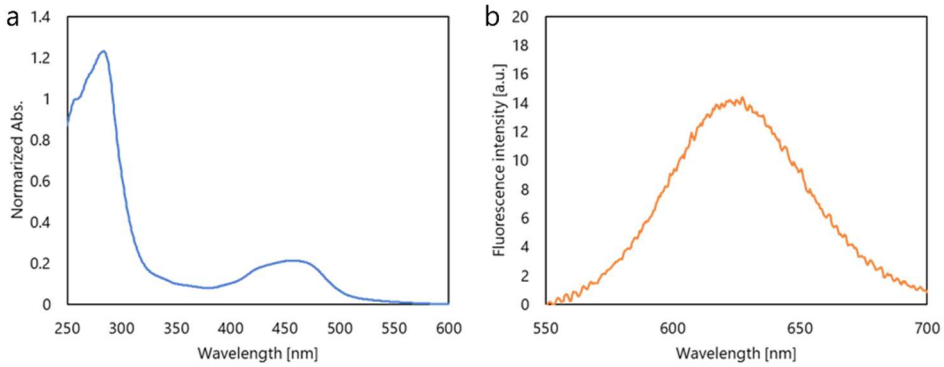

Figure 3-5. (a) Absorption spectrum and (b) emission spectrum of T6-Ru.

Conditions

NaCl = 100 mM

10mM phosphate buffer, pH = 7.0, 20°C

Excitation wavelength = 450 nm

In the absorption spectrum, an absorption peak originating from the MLCT of $Ru(bpy)_3$ was observed around 450 nm (Fig. 3-5a). In addition, emission at 620 nm, which is characteristic of $Ru(bpy)_3$, was observed in the emission spectrum (Fig. 3-5). This confirms that $Ru(bpy)_3$ was synthesized by the ligand exchange reaction in this study.

Two product peaks were observed by HPLC (Fig. 3-4). We expected these two products to be diastereomers in which Δ- $Ru(bpy)_3$ and Λ-$Ru(bpy)_3$ were introduced into DNA. Therefore, we separated each peak and measured the CD spectra.

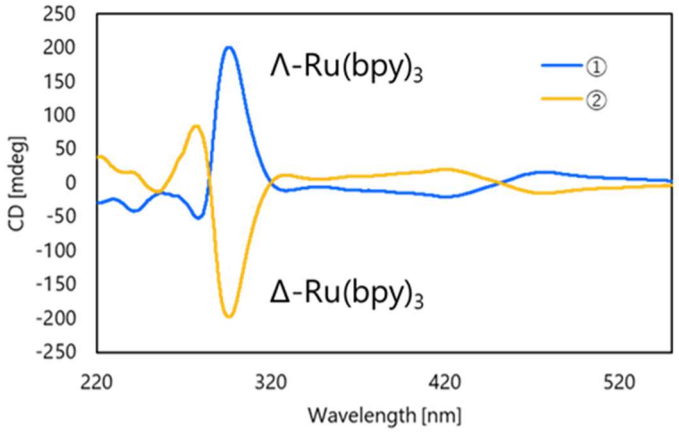

Figure 3-6. CD spectra of T6-Ru.

Conditions

NaCl = 100 mM

10mM phosphate buffer, pH = 7.0, 20°C

Each CD spectrum was observed with inverted positive and negative values (Fig. 3-6). In comparison with a previous report[16], the CD spectra revealed that the peak with the short elution time is DNA with Λ-$Ru(bpy)_3$ introduced and the peak with the long elution time is DNA with Δ-$Ru(bpy)_3$ introduced.

3-4-2 Ligand exchange reaction in ACGT mixed sequence

To investigate the energy transfer from pyrene to $Ru(bpy)_3$, ligand exchange reactions were performed with bpy- DNA conjugates of ACGT mixed sequences (ACGT-bpy). After the reaction,

mass spectrometry and HPLC purification were performed.

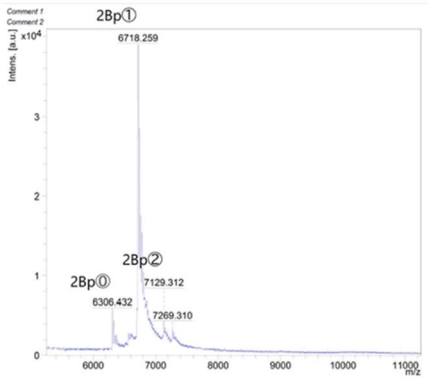

Figure 3-7. Mass spectrum of ACGT-bpy after reaction.

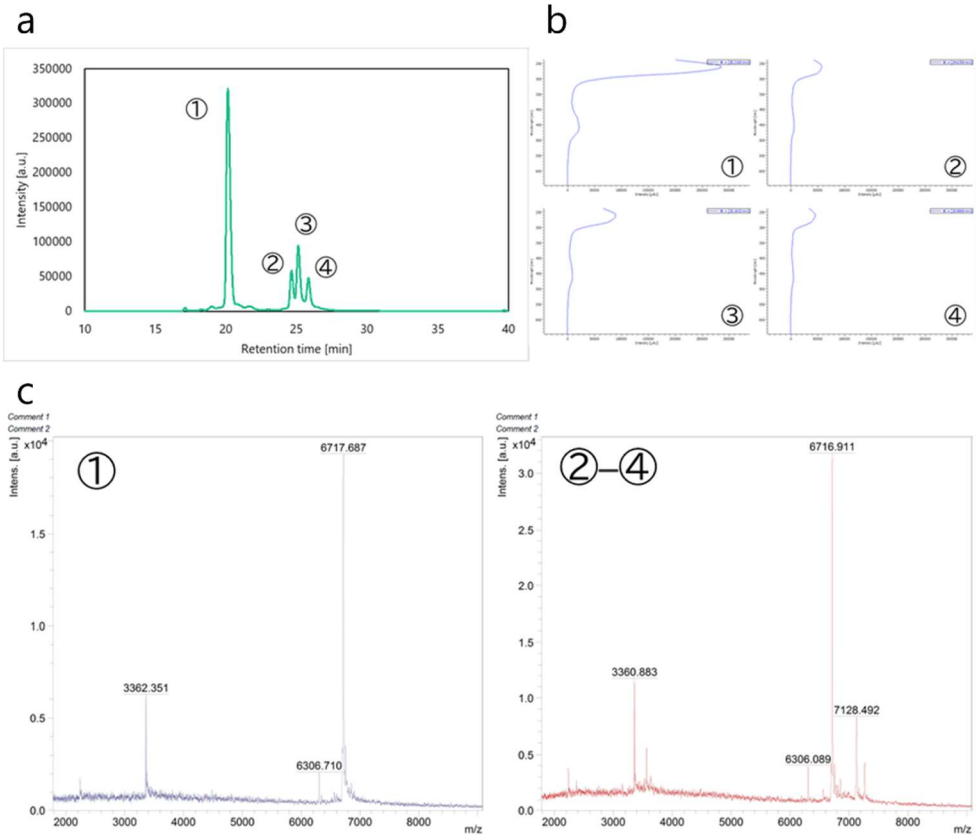

Figure 3-8. (a) HPLC profile of ACGT-bpy after reaction. (b) Absorption spectrum of each peak. (c) Mass spectrum of each peak.

Conditions

[DNA-bpy] = 1 mM, [$Ru(bpy)_2Cl_2$] = 2 mM, [NaCl] = 50 mM

Buffer: H_2O:MeOH = 1:1, 200μl, 80 °C

Molecular weight of the bpy-DNA conjugates, molecular weight of bpy-DNA conjugates (calculated mass = 6303.19, observed mass = 6306.432), that of Ru-DNA conjugates (calculated

mass = 6717.14, observed mass = 6718.259) and molecular weights greater than these conjugates were observed (Fig. 3-7). 2Bp② is consistent with the molecular weight of the molecule thought to have two $Ru(bpy)_2$ introduced (calculated mass = 7131.27). HPLC results showed that four peaks were observed (Fig. 3-8a). The first peak and the second to fourth peaks were separated and analyzed by mass spectrometry. The first peak showed the molecular weight of the target compound, whereas the second to fourth peaks showed the molecular weight of the target compound with two $Ru(bpy)_2$ introduced (Fig. 3-8c). These results suggest that the ACGT mixture sequence causes extra $Ru(bpy)_2$ to introduce.

3-4-3 Ligand exchange reaction at each base test sequence

Based on the previous results, we expected that other bases could bind to ruthenium. Therefore, test sequences other than T (A6-Bp, C6-Bp, G6-Bp) were synthesized and subjected to ligand exchange reactions under $Ru(bpy)_2$ excess conditions. Mass spectrometry was performed after the reaction. Note that G6-Bp could not be purified by HPLC, so it was used in the reaction as is after simple purification by PolyPac.

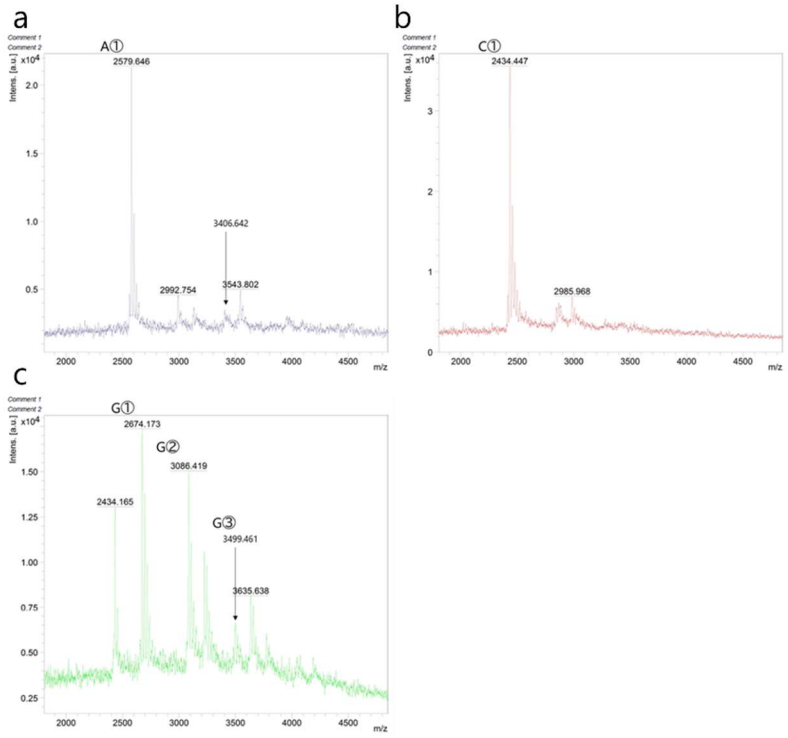

Figure 3-9. Mass spectrum of (a) A6-Bp, (b) C6-Bp and (c) G6-Bp after reaction.

Conditions

[DNA-bpy] = 0.1 mM, $[Ru(bpy)_2Cl_2]$ = 1 mM, [NaCl] = 50 mM

Buffer: H_2O:MeOH = 1:1, 200μl, 80 °C

In A6-Bp (Fig. 3-9a) and C6-Bp (Fig. 3-9b), no molecular weight with an excess of $Ru(bpy)_2$ was observed.

In contrast, molecular weights with one (G②: calculated mass = 3089.57, observed mass = 3086.419) or two (G③: calculated mass = 3503.61, observed mass = 3499.461) excess $Ru(bpy)_2$ bound were observed in G6-Bp (Fig. 3-9c). This suggests that DNA with a guanine-containing sequence produces a byproduct in the ligand exchange reaction.

3-4-4 Reaction verification of G and $Ru(bpy)_2Cl_2$

The previous results suggested that guanine reacts with $Ru(bpy)_2Cl_2$. Therefore, we performed the reaction under the same conditions as the ligand exchange reaction using a sequence in which a guanine was introduced into poly-T (T6-G).

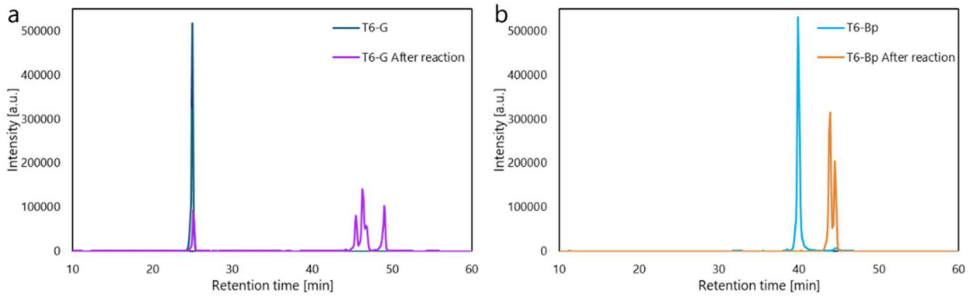

Figure 3-10. HPLC profiles of (a) T6-G and (b) T6-Bp after reaction.

Conditions

[DNA] = 0.1 mM, $[Ru(bpy)_2Cl_2]$ = 1 mM, [NaCl] = 50 mM

Buffer: H_2O:MeOH = 1:1, 200μl, 80 °C

After the reaction, multiple peaks with longer retention times than T6-G were observed (Fig. 3-10a). This indicates that $Ru(bpy)_2Cl_2$ reacts with guanine in some way. The change in retention time between T6-G and the product was larger than that observed in the ligand exchange reaction with T6-Bp (Fig. 3-10b). This confirms that of the two types of peaks observed during the ligand exchange reaction with the ACGT mixed sequence, the sharp large peak with the shorter retention time is the target product and the multiple small peaks with the longer retention time are by-products. The sequence was longer than the test sequence, which likely resulted in the diastereomers Δ-$Ru(bpy)_3$ and Λ-$Ru(bpy)_3$ not being separated and observed as a single peak.

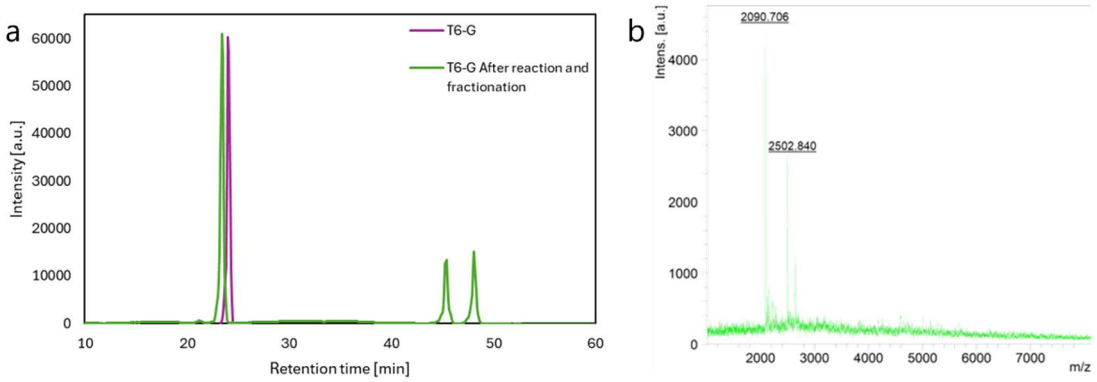

Figure 3-11. (a) HPLC profiles and (b) mass spectrum of T6-G1 after reaction and fractionation.

The products resulting from the T6-G1 ligand exchange reaction were fractionated. The products were returned to T6-G after fractionation(Fig. 3-11a). Mass spectrometry results showed the molecular weight of T6-G (calculated mass = 2505.41, observed mass = 2090.706) and that of T6-G combined with $Ru(bpy)_2Cl_2$ (calculated mass = 2505.41, observed mass = 2502.840) (Fig. 3-11b). This suggests that guanine reacts with $Ru(bpy)_2Cl_2$, but the product is unstable and can be destroyed by drying or other manipulations. In the ligand exchange reaction, the presence of guanine was found to produce a byproduct. In subsequent experiments, the sequence of the Ru-DNA complex was chosen not to include guanine.

3-4-5 Effect of the introduction of $Ru(bpy)_3$ on the structure of DNA

To investigate the effect of $Ru(bpy)_3$ incorporation on the structural stability of the DNA, melting temperature measurements were performed in duplex (3WJ_1 / 3WJ_1c and 3WJ_1 / 3WJ_1c-Ru) and 3-way junction (3WJ_1 / 3WJ_2 / 3WJ_3 and 3WJ_1 / 3WJ_2-Ru / 3WJ_3).

Table 3-1. Melting temperature of Duplex and 3WJ with and without $Ru(bpy)_3$

Name	*T*m	Δ*T*m
Duplex w/o $Ru(bpy)_3$	57.2	
Duplex w/ $Ru(bpy)_3$	52.7	-4.5
3WJ w/o $Ru(bpy)_3$	37.5	
3WJ w/ $Ru(bpy)_3$	40.9	3.5

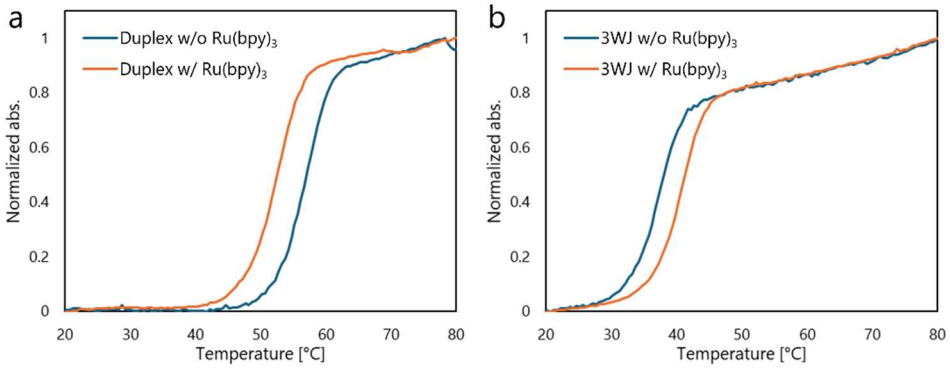

Figure 3-12. Melting profiles of (a) duplex and (b) 3-way junction.

Conditions

[DNA] = 1.0 μM, [NaCl] = 100 mM

10 mM phosphate buffer, pH = 7.0

The introduction of $Ru(bpy)_3$ into the duplex chain decreased the T_m by about 4.5°C (Fig. 3-12a). This indicates that the introduction of $Ru(bpy)_3$ into the duplex chain destabilizes the structure. This indicates that the introduction of $Ru(bpy)_3$ into the duplex destabilizes the duplex. In contrast, the introduction of $Ru(bpy)_3$ into the 3-way junction increased T_m by about 3.3°C (Fig. 3-12b). This indicates that the introduction of $Ru(bpy)_3$ into the center of the 3-way junction stabilizes the structure. This indicates that the introduction of $Ru(bpy)_3$ into the center of the 3-way junction stabilizes the structure. $Ru(bpy)_3$ is thought to promote the formation of DNA structures because of its positive charge. On the other hand, $Ru(bpy)_3$ is considered to inhibit the formation of DNA duplexes because of its bulkiness, but it does not inhibit the formation of DNA junction because there is enough space in the center of DNA junction.

3-4-6 Verification of energy transfer from pyrene to $Ru(bpy)_3$

In order to verify whether energy is transferred from pyrene to $Ru(bpy)_3$ in the Förste type, emission spectra and excitation spectra of $Ru(bpy)_3$ were measured at the duplex (3WJ_1-Py / 3WJ_1c and 3WJ_1-Py / 3WJ_1c-Ru) and 3-way junction (3WJ_1-Py / 3WJ_2 / 3WJ_3 and 3WJ_1-Py / 3WJ_2-Ru / 3WJ_3). The distance between Pyrene and $Ru(bpy)_3$ is 4 bp.

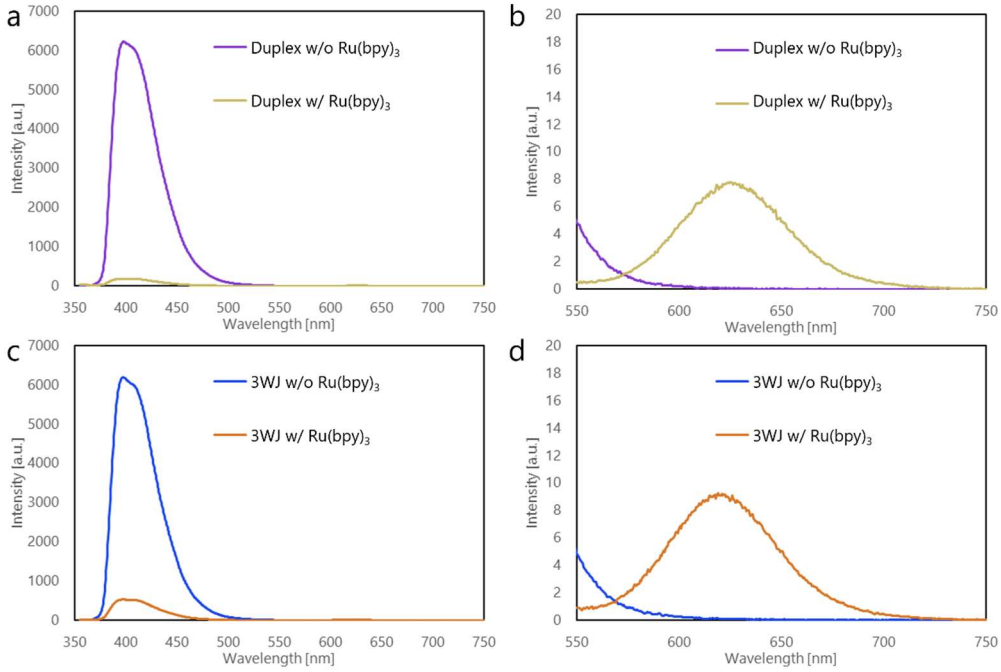

Figure 3-13. (a) Emission spectra of duplex. (b) Emission spectra of duplex expanded $Ru(bpy)_3$ region. (c) Emission spectra of 3-way junction. (b) Emission spectra of 3-way junction expanded $Ru(bpy)_3$ region.

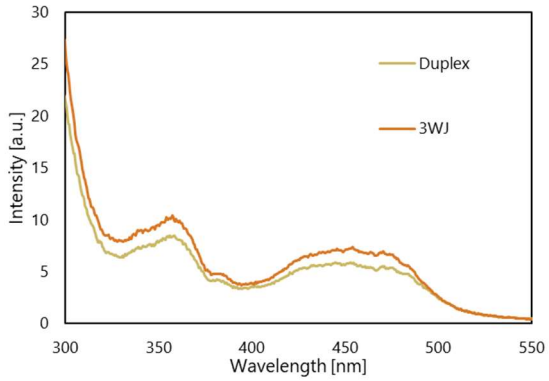

Figure 3-14. Excitation spectra of duplex and 3-way junction.

Conditions

[DNA_1-1] = 0.5 μM, [DNA_1-1c or DNA_1-2] = 1.0 μM, [DNA_1-3] = 1.5 μM, [NaCl] = 100 mM

10 mM phosphate buffer, pH = 7.0, 20°C

Excitation = 345 nm, Emission = 620 nm

In both duplex (Fig. 3-13a) and 3-way junction (Fig. 3-13c), the introduction of $Ru(bpy)_3$ greatly reduced the fluorescence of pyrene, confirming a highly efficient energy transfer from pyrene to $Ru(bpy)_3$. The FRET efficiency was 0.97 for the duplex and 0.90 for the 3-way junction.

A small amount of $Ru(bpy)_3$ emission was also observed (Fig.3-13b, d). In excitation spectra of both the duplex and 3-way junction, when pyrene was introduced, a peak similar in shape to the absorption spectrum of pyrene was observed in the absorption region of pyrene (Fig. 3-14). This confirms that the energy transfer from pyrene to $Ru(bpy)_3$ is as designed.

3-4-7 Energy transfer efficiency depending only on distance

We tested whether the energy transfer from pyrene depends only on distance when $Ru(bpy)_3$ is used as an acceptor. pyrene was introduced as a donor at the duplex site of the 3-way junction and $Ru(bpy)_3$ was placed in the center as an acceptor. The base pairing between the donor and acceptor was varied from 0 bp to 19 bp. For comparison, an organic fluorophore, perylene, was placed in the center of the 3-way junction as an acceptor and was also studied in the same way. The combinations of DNA strand are shown in Table S2. Steady-state fluorescence spectra were measured at each distance. FRET efficiencies were calculated from the percentage decrease in donor emission due to the introduction of acceptors.

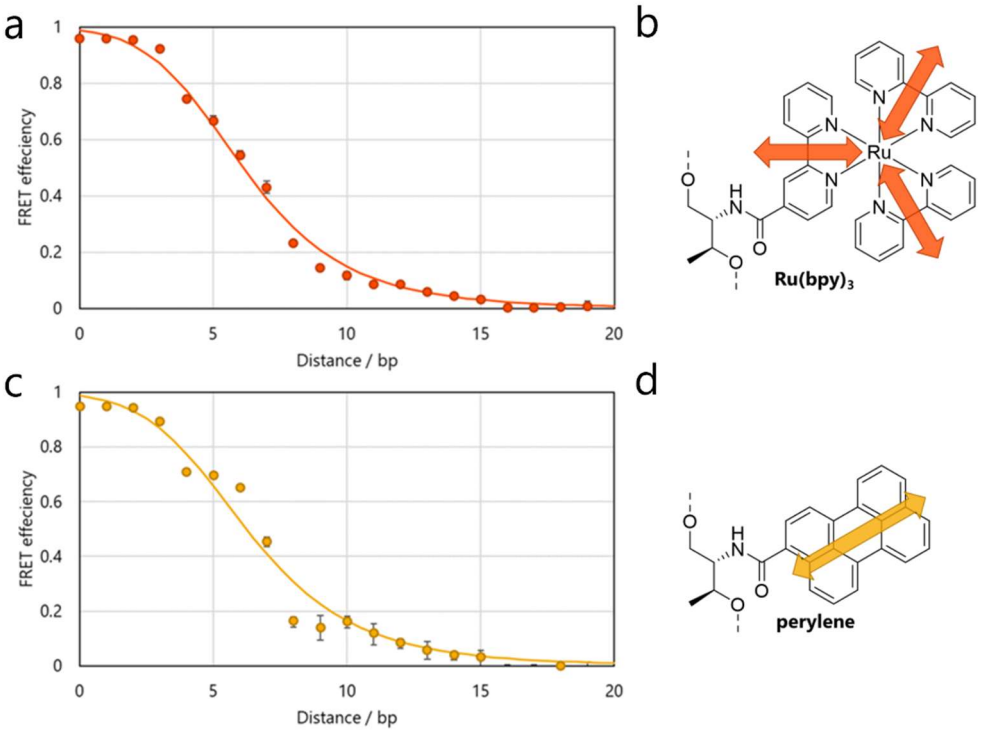

Figure 3-15. (a) FRET efficiencies from pyrene to $Ru(bpy)_3$. (b) Transition dipole moments of $Ru(bpy)_3$. (c) FRET efficiencies from pyrene to perylene. (b) Transition dipole moment of perylene.

Conditions

[DNA-Py] = 0.5 μM, [DNA-Ac] = 1.0 μM, [DNA-N] = 1.5 μM, [NaCl] = 100 mM

10mM phosphate buffer, pH = 7.0, 20°C

Excitation wavelength = 345 nm

When $Ru(bpy)_3$ was used as an acceptor, the curve was in excellent agreement with the theoretical curve when the orientations were averaged (Fig. 3-15a). This may be due to the symmetry of the transition dipole moments of $Ru(bpy)_3$ canceling the orientation dependence of the FRET, as designed. In contrast, a slight orientation dependence was observed when perylene was used as an acceptor (Fig. 3-15c). Thus, it is shown that the introduction of $Ru(bpy)_3$ as FRET acceptor at the DNA junction can construct an orientation-independent FRET system.

3-4-8 Modeling

Next, we modeled a 3-way junction with $Ru(bpy)_3$ from the fitting of the theoretical curve. The crystal structure of the 3-way junction (PDB: 1DRG[17]) was modified to introduce $Ru(bpy)_3$, and the position of $Ru(bpy)_3$ was determined from fitting the theoretical curve of Pyrene-$Ru(bpy)_3$ FRET and calculated as the initial structure. The structure of $Ru(bpy)_3$ was obtained as if it were positioned perpendicular to the 3-way junction plane (Fig. 3-16).

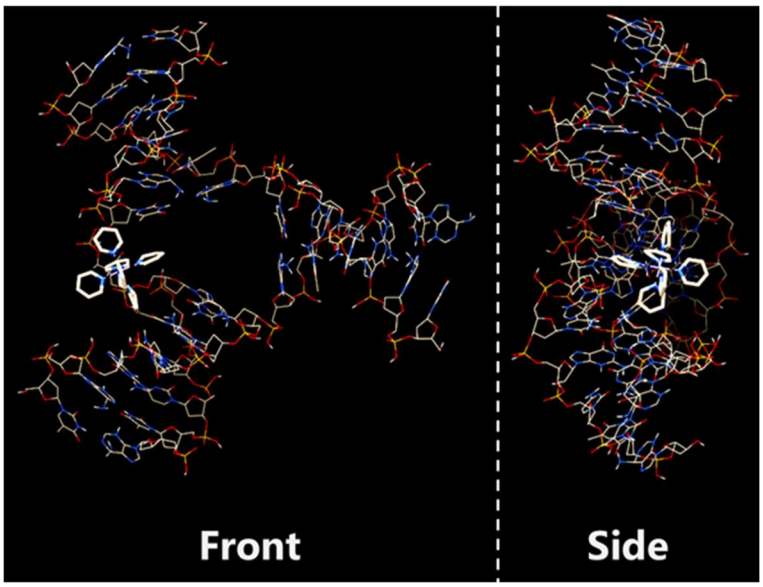

Figure 3-16. Modeling of the DNA 3-way junction with $Ru(bpy)_3$ in the center.

3-5 Conclusion

In this study we developed a novel distance-only dependent FRET system by using $Ru(bpy)_3$ with transition dipole moments in spatially symmetric orientations. A novel bpy monomer was designed to synthesize $Ru(bpy)_3$-DNA conjugate, and the bpy-DNA complex was synthesized using general DNA synthesis method. $Ru(bpy)_3$-DNA conjugate was synthesized by ligand exchange reaction of bpy-DNA conjugate and $Ru(bpy)_2Cl_2$. Since byproducts were observed in the ligand exchange reaction with bpy-DNA conjugate, which has guanine in the sequence, the

sequence of $Ru(bpy)_3$-DNA conjugate should not contain guanine. The introduction of $Ru(bpy)_3$ destabilized the DNA duplex and stabilized DNA 3WJ. Highly efficient FRET from pyrene to $Ru(bpy)_3$ were observed in the DNA structures. FRET from pyrene to $Ru(bpy)_3$ in 3WJ was orientation independent. This system can be used for a nano-ruler or a simplification of complex energy transfer systems.

3-6 Experimental section

Materials

All conventional phosphoramidite monomers, CPG columns, reagents for DNA synthesis, and Poly-Pak II cartridges were purchased from Glen Research. Other reagents for the synthesis of phosphoramidite monomers and *cis*-Dichlorobis(2,2'-bipyridine) ruthenium(II) were purchased from Tokyo Chemical Industry, Wako, and Aldrich. Native oligonucleotides were purchased from Integrated DNA Technologies. Monomers tethering a bipyridine unit were synthesized as described below. Modified oligomers were synthesized by employing these phosphoramidite monomers and standard DNA monomers on an automated DNA synthesizer (M-6-MX, Nihon Techno Service). Oligomers were purified by reversed-phase HPLC and characterized by MALDI-TOF MS (Autoflex maX, Bruker) and HPLC.

Synthesis of Ru-DNA conjugates

DNAs conjugated to the Ru complex were synthesized by the ligand exchange reaction of *cis*-dichlorobis(2,2'-bipyridine) ruthenium(II) and DNA tethering a bipyridine moiety. Bipyridine-modified DNA strands (0.2 μmol, final concentration 1 mM) were dissolved in a 1:1 mixture of methanol and 100 mM aqueous NaCl solution in the presence of 2 mM *cis*-dichlorobis(2,2'-bipyridine) ruthenium(II) (total volume 200 μl). After 6 h of incubation at 80 ºC, products were purified by reversed-phase HPLC and characterized by MALDI-TOF MS (Autoflex maX, Bruker) and HPLC.

HPLC analyses

A Mightysil RP-18GP II column (Kanto Chemical Co., Inc.) was used for HPLC analyses. The flow rate was 0.5 mL min^{-1}. Absorbance was monitored at 260 nm. Spectra of peaks at each retention time were recorded on JASCO EXTREMA HPLC system.

Circular dichroism (CD) measurements

CD spectra were measured on a JASCO model J-820 equipped with a programmable temperature controller using 10-mm quartz cells. Spectra were measured at 20 ºC. The sample solutions contained 100 mM NaCl, 10 mM phosphate buffer (pH 7.0).

Measurement of absorption spectra and melting temperatures

Absorption spectra were measured on a V-730 (JASCO). The sample solutions contained 100 mM NaCl, 10 mM phosphate buffer (pH 7.0). Absorption spectra were measured at 20 °C after annealing at 80 ºC. The melting curves were measured with a UV-1800 (Shimadzu) by monitoring 260 nm absorbance versus temperature. The melting temperature (T_m) was determined from the maximum value in the first derivative of the heating curve. The temperature ramp was 0.5 °C min^{-1}. The sample solutions contained 100 mM NaCl, 10 mM phosphate buffer (pH 7.0).

Emission measurements

Emission spectra were measured on JASCO model FP-8500. Band widths were 2.5 nm for excitation and emission. Before measurements, sample solutions were heated at 80 °C, then slowly cooled to 20 °C at a rate of 1 °C min^{-1}. Emission spectra were measured at 20 °C. The sample solutions contained 100 mM NaCl, 10 mM phosphate buffer (pH 7.0).

Synthesis of phosphoramidite monomer tethering bipyridine

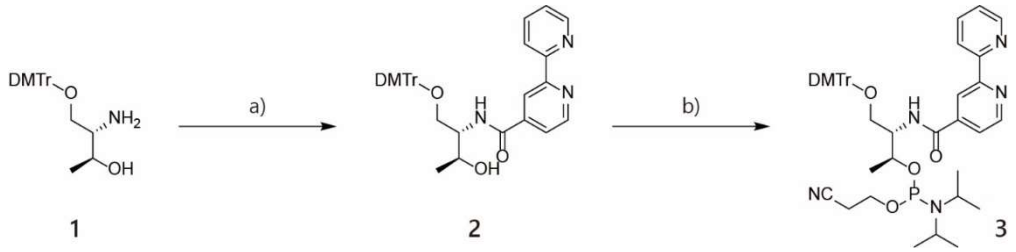

Scheme S3-1. Synthesis of phosphoramidite tethering bipyridine. Reagents and conditions: a) [2,2′-bipyridine]-4-carboxylic acid, DMT-MM, Et_3N, DMF, room temperature, 12 h, 56%; b) $(iPr)_2NP(Cl)(OCH_2CH_2CN)$, Et_3N, dryCH_2Cl_2, 0 ºC, 2 h, 70%.

Compound 2. Compound **1** and [2,2'-bipyridine]-4-carboxylic acid were synthesized as described previously. To a stirred solution of [2,2'-bipyridine]-4-carboxylic acid (0.49 g, 2.4 mmol) and triethylamine (1.69 mL, 12.1 mmol) in DMF (50 mL) were added compound **1** (2.7 mmol) and DMT-MM (1.01 g, 3.7 mmol). After stirring at room temperature for 12 h, $CHCl_3$ was added to the reaction mixture. The mixture was washed with saturated $NaHCO_3$ (twice) and brine (twice) and dried over $MgSO_4$. The solvent was removed by evaporation. Silica gel column chromatography (hexanes:AcOEt, 1:4 (v/v) and 3% triehtylamine) afforded compound **2** as a white solid (0.80 g, yield 56%).

^{1}H-NMR [$CDCl_3$, 500 MHz] δ = 8.80 (dd, J = 5, 1 Hz, 1H), 8.70 (d, J = 2 Hz, 1H), 8.68-8.67 (m, 1H), 8.43-8.41 (m, 1H), 7.83 (ddd, J = 15, 2, 2 Hz, 1H), 7.71 (dd, J = 5, 2 Hz, 1H), 7.41-7.40

(m, 2H), 7.35-7.28 (m, 7H), 7.21-7.18 (m, 1H), 7.05 (d, J = 9 Hz, 1H), 6.80 (ddd, J = 9, 7, 7 Hz, 4H), 4.28-4.25 (m, 1H), 4.20-4.16 (m, 1H), 3.75 and 3.73 (s, 6H), 3.55 (dd, J = 10, 5 Hz, 1H), 3.41 (dd, J = 10, 4 Hz, 1H), 3.13 (d, J = 3 Hz, 1H), 1.23 (d, J = 7 Hz, 3H). ^{13}C-NMR [$CDCl_3$, 126 MHz] δ = 166.1, 158.8, 157.2, 155.4, 150.2, 149.4, 144.5, 142.7, 137.2, 135.5, 130.1, 128.2, 128.0, 127.2, 124.3, 121.6, 121.4, 117.8, 113.5, 87.0, 68.5, 65.1, 55.3, 54.4, 20.3. HRMS(FAB) calcd for $C_{36}H_{35}N_3O_5$ (M^+) 589.2577. Found 589.2490.

Compound 3. In 20 mL of dry dichloromethane under nitrogen, compound **2** (0.8 g, 1.4 mmol) and triethylamine (0.94 mL, 6.8 mmol) were reacted with 2-cyanoethyl diisopropylchlorophosphoramidite (0.45 mL, 2.0 mmol) at 0 ºC. After 1 h, the solvent was removed by evaporation. Silica gel column chromatography (hexanes:AcOEt, 1:1 (v/v) and 3% triehtylamine) afforded compound **3** as a white solid (0.76 g, yield 71%).

^{31}P-NMR [202 MHz, $CDCl_3$] δ =148.4, 147.9.

3-7 References

1. Kennard, O.; Hunter, W. N., Single-Crystal X-Ray Diffraction Studies of Oligonucleotides and Oligonucleotide–Drug Complexes. *Angewandte Chemie International Edition in English* **1991,** *30* (10), 1254-1277.
2. Carugo, O.; Carugo, K. D., When X-rays modify the protein structure: radiation damage at work. *Trends in Biochemical Sciences* **2005,** *30* (4), 213-219.
3. Robinson, C. V.; Sali, A.; Baumeister, W., The molecular sociology of the cell. *Nature* **2007,** *450* (7172), 973-982.
4. Alnabati, E.; Kihara, D. Advances in Structure Modeling Methods for Cryo-Electron Microscopy Maps *Molecules* [Online], 2020.
5. Förster, T., Zwischenmolekulare Energiewanderung und Fluoreszenz. *Annalen der Physik* **1948,** *437* (1-2), 55-75.
6. Komatsu, N.; Aoki, K.; Yamada, M.; Yukinaga, H.; Fujita, Y.; Kamioka, Y.; Matsuda, M., Development of an optimized backbone of FRET biosensors for kinases and GTPases. *Molecular Biology of the Cell* **2011,** *22* (23), 4647-4656.
7. Regot, S.; Hughey, Jacob J.; Bajar, Bryce T.; Carrasco, S.; Covert, Markus W., High-Sensitivity Measurements of Multiple Kinase Activities in Live Single Cells. *Cell* **2014,** *157* (7), 1724-1734.
8. Johnson-Buck, A.; Su, X.; Giraldez, M. D.; Zhao, M.; Tewari, M.; Walter, N. G., Kinetic fingerprinting to identify and count single nucleic acids. *Nature Biotechnology* **2015,** *33* (7), 730-732.
9. Cai, S.; Deng, Y.; Fu, S.; Li, J.; Yu, C.; Su, X., Single-molecule dynamic DNA

junctions for engineering robust molecular switches. *Chemical Science* **2019,** *10* (43), 9922-9927.
10. Kuchimaru, T.; Suka, T.; Hirota, K.; Kadonosono, T.; Kizaka-Kondoh, S., A novel injectable BRET-based in vivo imaging probe for detecting the activity of hypoxia-inducible factor regulated by the ubiquitin-proteasome system. *Scientific Reports* **2016,** *6* (1), 34311.
11. Yang, J.; Cumberbatch, D.; Centanni, S.; Shi, S.-q.; Winder, D.; Webb, D.; Johnson, C. H., Coupling optogenetic stimulation with NanoLuc-based luminescence (BRET) Ca++ sensing. *Nature Communications* **2016,** *7* (1), 13268.
12. Kawamoto, K.; Tamiya, Y.; Storr, T.; Cogdell, R. J.; Kinoshita, I.; Hashimoto, H., Disentangling the 1MLCT transition of [Ru(bpy)3]2+ by Stark absorption spectroscopy. *Journal of Photochemistry and Photobiology A: Chemistry* **2018,** *353*, 618-624.
13. Fujii, T.; Kashida, H.; Asanuma, H., Analysis of Coherent Heteroclustering of Different Dyes by Use of Threoninol Nucleotides for Comparison with the Molecular Exciton Theory. *Chemistry – A European Journal* **2009,** *15* (39), 10092-10102.
14. Baron, A.; Herrero, C.; Quaranta, A.; Charlot, M.-F.; Leibl, W.; Vauzeilles, B.; Aukauloo, A., Efficient electron transfer through a triazole link in ruthenium(ii) polypyridine type complexes. *Chemical Communications* **2011,** *47* (39), 11011-11013.
15. Vasta, J. D.; Raines, R. T., Human Collagen Prolyl 4-Hydroxylase Is Activated by Ligands for Its Iron Center. *Biochemistry* **2016,** *55* (23), 3224-3233.
16. Oppermann, M.; Bauer, B.; Rossi, T.; Zinna, F.; Helbing, J.; Lacour, J.; Chergui, M., Ultrafast broadband circular dichroism in the deep ultraviolet. *Optica* **2019,** *6* (1), 56-60.
17. Woods, K. C.; Martin, S. S.; Chu, V. C.; Baldwin, E. P., Quasi-equivalence in site-specific recombinase structure and function: crystal structure and activity of trimeric cre recombinase bound to a three-way lox DNA junction11Edited by K. Morikawa. *Journal of Molecular Biology* **2001,** *313* (1), 49-69.

3-8 Appendixes

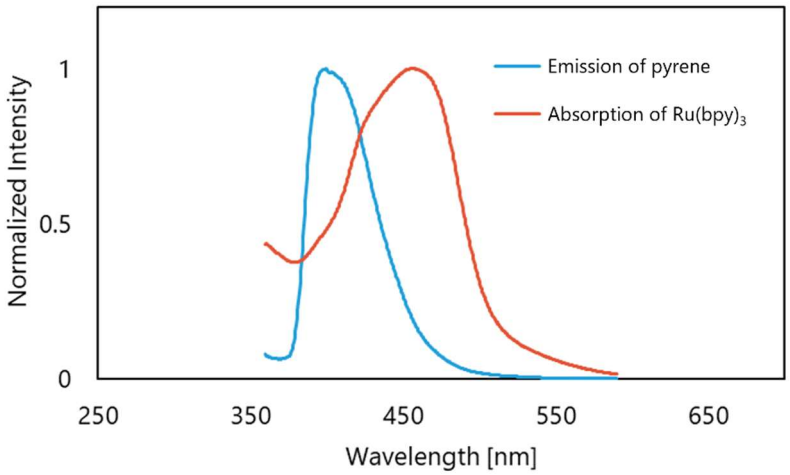

Figure S3-1. Overlap between the emission spectrum of Pyrene and the absorption spectrum of $Ru(bpy)_3$

Table S3-1. DNA sequence

name	Sequence (5'→3')
T6-Bp	TTTBpTTT
A-6Bp	AAABpAAA
C6-Bp	CCCBpCCC
G6-Bp	GGGBpGGG
ACGT-Bp	CCATTACAACBpTCCCGTCACT
T6-G	TTTGTTT
T6-Ru	TTTRuTTT
A-6Ru	AAARuAAA
C6-Ru	CCCRuCCC
G6-Ru	GGGRuGGG
ACGT-Ru	CCATTACAACRuTCCCGTCACT
T6-G	TTTGTTT
3WJ_1	GTGTAAATGTGTTGTAATGG
3WJ_1-Py	GTGTAAPyATGTGTTGTAATGG
3WJ_2	CCATTACAACTCCCCTCACT
3WJ_2-Bp	CCATTACAACBpTCCCCTCACT
3WJ_2-Ru	CCATTACAACRuTCCCCTCACT
3WJ_3	AGTGAGGGGAACATTTACAC
3WJ_1c-Bp	CCATTACAACBpACATTTACAC
3WJ_1c-Ru	CCATTACAACRuACATTTACAC
3WJ-Py00	CTCCGAATCTATTATCCAAGCAPyAAAGTGTATGTGA
3WJ-Py04	CTCCGAATCTATTATCCAPyAGCAAAAGTGTATGTGA
3WJ-Py08	CTCCGAATCTATTAPyTCCAAGCAAAAGTGTATGTGA
3WJ-Py12	CTCCGAATCTPyATTATCCAAGCAAAAGTGTATGTGA
3WJ-Py16	CTCCGAPyATCTATTATCCAAGCAAAAGTGTATGTGA
3WJ-Ru00	TCACATACACTTTRuCCTACTCTCA
3WJ-Ru01	TCACATACACTTRuCCTACTCTCA
3WJ-Ru02	TCACATACACTRuCAACTACCTC
3WJ-Ru03	TCACATACACRuCCTACTCTCA
3WJ-E00	TCACATACACTTTECCTACTCTCA
3WJ-E01	TCACATACACTTECCTACTCTCA
3WJ-E02	TCACATACACTECAACTACCTC
3WJ-E03	TCACATACACECCTACTCTCA
3WJ-N00	TCACATACACTTTCCTACTCTCA
3WJ-N01	TCACATACACTTCCTACTCTCA
3WJ-N02	TCACATACACTCAACTACCTC
3WJ-N03	TCACATACACCCTACTCTCA
3WJ-n00	TGAGAGTAGGTGCTTGGATAATAGATTCGGAG
3WJ-n01	TGAGAGTAGGTTGCTTGGATAATAGATTCGGAG
3WJ-n02	GAGGTAGTTGTTTGCTTGGATAATAGATTCGGAG
3WJ-n03	TGAGAGTAGGTTTTGCTTGGATAATAGATTCGGAG

Bp: bpy, Ru: $Ru(bpy)_3$, Py: pyrene, E: perylene

Table S3-2. DNA combinations forming 3WJ

distance	name	sequence				
0	3WJ-Py00	5'-	CTCCGAATCTATTATCCAAGCAPy		AAAGTGTATGTGA	-3'
	3WJ-Ac00	5'-	TCACATACACTTT	Ac	CCTACTCTCA	-3'
	3WJ-N00	5'-	TGAGAGTAGG		TGCTTGGATAATAGATTCGGAG	-3'
1	3WJ-Py00	5'-	CTCCGAATCTATTATCCAAGCAPyA		AAGTGTATGTGA	-3'
	3WJ-Ac01	5'-	TCACATACACTT	Ac	CCTACTCTCA	-3'
	3WJ-N01	5'-	TGAGAGTAGG		TTGCTTGGATAATAGATTCGGAG	-3'
2	3WJ-Py00	5'-	CTCCGAATCTATTATCCAAGCAPyAA		AGTGTATGTGA	-3'
	3WJ-Ac02	5'-	TCACATACACT	Ac	CAACTACCTC	-3'
	3WJ-N02	5'-	GAGGTAGTTG		TTTGCTTGGATAATAGATTCGGAG	-3'
3	3WJ-Py00	5'-	CTCCGAATCTATTATCCAAGCAPyAAA		GTGTATGTGA	-3'
	3WJ-Ac03	5'-	TCACATACAC	Ac	CCTACTCTCA	-3'
	3WJ-N03	5'-	TGAGAGTAGG		TTTTGCTTGGATAATAGATTCGGAG	-3'
4	3WJ-Py04	5'-	CTCCGAATCTATTATCCAPyAGCA		AAAGTGTATGTGA	-3'
	3WJ-Ac00	5'-	TCACATACACTTT	Ac	CCTACTCTCA	-3'
	3WJ-N00	5'-	TGAGAGTAGG		TGCTTGGATAATAGATTCGGAG	-3'
5	3WJ-Py04	5'-	CTCCGAATCTATTATCCAPyAGCAA		AAGTGTATGTGA	-3'
	3WJ-Ac01	5'-	TCACATACACTT	Ac	CCTACTCTCA	-3'
	3WJ-N01	5'-	TGAGAGTAGG		TTGCTTGGATAATAGATTCGGAG	-3'
6	3WJ-Py04	5'-	CTCCGAATCTATTATCCAPyAGCAAA		AGTGTATGTGA	-3'
	3WJ-Ac02	5'-	TCACATACACT	Ac	CAACTACCTC	-3'
	3WJ-N02	5'-	GAGGTAGTTG		TTTGCTTGGATAATAGATTCGGAG	-3'
7	3WJ-Py04	5'-	CTCCGAATCTATTATCCAPyAGCAAAA		GTGTATGTGA	-3'
	3WJ-Ac03	5'-	TCACATACAC	Ac	CCTACTCTCA	-3'
	3WJ-N03	5'-	TGAGAGTAGG		TTTTGCTTGGATAATAGATTCGGAG	-3'
8	3WJ-Py08	5'-	CTCCGAATCTATTAPyTCCAAGCA		AAAGTGTATGTGA	-3'
	3WJ-Ac00	5'-	TCACATACACTTT	Ac	CCTACTCTCA	-3'
	3WJ-N00	5'-	TGAGAGTAGG		TGCTTGGATAATAGATTCGGAG	-3'
9	3WJ-Py08	5'-	CTCCGAATCTATTAPyTCCAAGCAA		AAGTGTATGTGA	-3'
	3WJ-Ac01	5'-	TCACATACACTT	Ac	CCTACTCTCA	-3'
	3WJ-N01	5'-	TGAGAGTAGG		TTGCTTGGATAATAGATTCGGAG	-3'
10	3WJ-Py08	5'-	CTCCGAATCTATTAPyTCCAAGCAAA		AGTGTATGTGA	-3'
	3WJ-Ac02	5'-	TCACATACACT	Ac	CAACTACCTC	-3'
	3WJ-N02	5'-	GAGGTAGTTG		TTTGCTTGGATAATAGATTCGGAG	-3'

11	3WJ-Py08	5'-	CTCCGAATCTATTAPyTCCAAGCAAAA		GTGTATGTGA	-3'
	3WJ-Ac03	5'-	TCACATACAC	Ac	CCTACTCTCA	-3'
	3WJ-N03	5'-	TGAGAGTAGG		TTTTGCTTGGATAATAGATTCGGAG	-3'
12	3WJ-Py12	5'-	CTCCGAATCTPyATTATCCAAGCA		AAAGTGTATGTGA	-3'
	3WJ-Ac00	5'-	TCACATACACTTT	Ac	CCTACTCTCA	-3'
	3WJ-N00	5'-	TGAGAGTAGG		TGCTTGGATAATAGATTCGGAG	-3'
13	3WJ-Py12	5'-	CTCCGAATCTPyATTATCCAAGCAA		AAGTGTATGTGA	-3'
	3WJ-Ac01	5'-	TCACATACACTT	Ac	CCTACTCTCA	-3'
	3WJ-N01	5'-	TGAGAGTAGG		TTGCTTGGATAATAGATTCGGAG	-3'
14	3WJ-Py12	5'-	CTCCGAATCTPyATTATCCAAGCAAA		AGTGTATGTGA	-3'
	3WJ-Ac02	5'-	TCACATACACT	Ac	CAACTACCTC	-3'
	3WJ-N02	5'-	GAGGTAGTTG		TTTGCTTGGATAATAGATTCGGAG	-3'
15	3WJ-Py12	5'-	CTCCGAATCTPyATTATCCAAGCAAAA		GTGTATGTGA	-3'
	3WJ-Ac03	5'-	TCACATACAC	Ac	CCTACTCTCA	-3'
	3WJ-N03	5'-	TGAGAGTAGG		TTTTGCTTGGATAATAGATTCGGAG	-3'
16	3WJ-Py16	5'-	CTCCGAPyATCTATTATCCAAGCA		AAAGTGTATGTGA	-3'
	3WJ-Ac00	5'-	TCACATACACTTT	Ac	CCTACTCTCA	-3'
	3WJ-N00	5'-	TGAGAGTAGG		TGCTTGGATAATAGATTCGGAG	-3'
17	3WJ-Py16	5'-	CTCCGAPyATCTATTATCCAAGCAA		AAGTGTATGTGA	-3'
	3WJ-Ac01	5'-	TCACATACACTT	Ac	CCTACTCTCA	-3'
	3WJ-N01	5'-	TGAGAGTAGG		TTGCTTGGATAATAGATTCGGAG	-3'
18	3WJ-Py16	5'-	CTCCGAPyATCTATTATCCAAGCAAA		AGTGTATGTGA	-3'
	3WJ-Ac02	5'-	TCACATACACT	Ac	CAACTACCTC	-3'
	3WJ-N02	5'-	GAGGTAGTTG		TTTGCTTGGATAATAGATTCGGAG	-3'
19	3WJ-Py16	5'-	CTCCGAPyATCTATTATCCAAGCAAAA		GTGTATGTGA	-3'
	3WJ-Ac03	5'-	TCACATACAC	Ac	CCTACTCTCA	-3'
	3WJ-N03	5'-	TGAGAGTAGG		TTTTGCTTGGATAATAGATTCGGAG	-3'

Py: pyrene, Ac: $Ru(bpy)_3$ or perylene or none

Capter 4 Visible light cross-linking of DNA duplexes using $Ru(bpy)_3$-introduced TFO (Dexter energy transfer from metal complex to dye)

4-1 Abstract

We developed a novel visible-light responsive system for site-selective cross-linking of DNA duplexes. DNA duplexes with stilbene pairs and TFO with $Ru(bpy)_3$ to form triplex with stilbene pairs and $Ru(bpy)_3$ in proximity. When this triplex is irradiated with visible light, the [2+2] cycloaddition of stilbene is catalyzed by $Ru(bpy)_3$, resulting in cross-linking of the DNA duplex. Energy calculations indicate that the DNA duplex is cross-linked by TTET from $Ru(bpy)_3$ to stilbene. DNA duplexes were not cross-linked unless stilbene and $Ru(bpy)_3$ were in proximity. It was shown that the cross-linking sites of DNA duplexes with stilbene pairs in two locations can be precisely controlled by the sequence of TFO. The system does not require orthogonal photoreactive molecules, making it applicable to complex photoresponsive circuits and nanomachines.

4-2 Introduction

Artificial control of biomolecular functions by external stimuli is a major goal of biotechnology. Light irradiation is an excellent external stimulus because it is easily controlled spatiotemporally and does not contaminate the reaction system. Orthogonal activation is possible by changing the excitation wavelength of photoresponsive molecules. Orthogonal light control systems that respond at different wavelengths are being studied challengingly in various fields as to biotechnology [1 2 3].

Controlling DNA function through photostimulation is an important tool for DNA nanotechnology and nucleic acid drug. Various light-responsive DNA systems have been reported by using photoisomerization [4 5], photocycloaddition [6 7], and photocaged bases [8 9]. Generally, for orthogonal light control, the chemical structure of the photoresponsive molecule is changed to change the wavelength at which it responds. Our laboratory also reported a system that responds to visible light by modifying the chemical structure of stilbene, which responds to ultraviolet light [10], and a photoresponsive system that orthogonally controls the stability of artificial nucleic acids by using two types of photoresponsive molecules with modified chemical structures [11]. Generally, the overlap in excitation wavelengths makes it difficult to construct photoresponsive systems that combine molecules responsive to multiple different wavelengths. Therefore, new strategies are needed for the development of orthogonal light-response systems.

In this study, we developed a novel photoresponsive system using photocatalyst. Tris(2,2′ -

bipyridine) ruthenium(II) ($Ru(bpy)_3$) was selected as a photocatalyst. DNA-Ru complex conjugates have been used for electron transfer [12], fluorescence probe [13] and nucleic acid drug [14]. Ru complexes are known to catalyze [2+2] cycloaddition reactions upon visible light irradiation [15]. We expected $Ru(bpy)_3$ to catalyze the [2+2] cycloaddition of stilbene within the DNA duplex, resulting in cross-linking of the DNA duplex.

4-3 Design

The purpose of this study is to cross-link DNA duplexes with visible light using triplex forming oligonucleotide (TFO) introduced $Ru(bpy)_3$ via D-threoninol. The design is shown in Fig. 4-1. Two stilbenes are introduced into the DNA duplex at complementary positions via D-threoninol. As a result, stilbenes form H-aggregates within the DNA Duplex. Since stilbene does not absorb visible light, irradiation with visible light does not cross-link this DNA duplex. By mixing this duplex with TFO with $Ru(bpy)_3$ at the end, the DNA triplex is formed in which the stilbene pair and the $Ru(bpy)_3$ are in close proximity. Irradiation of the DNA triplex with visible light excites $Ru(bpy)_3$, which transfers energy to the stilbene, resulting in [2+2] cycloaddition of the stilbene pair. Finally, DNA duplexes are cross-linked and thermally stabilized. By using this design, site-selective cross-linking of DNA duplexes can be expected, depending on the position of $Ru(bpy)_3$ introduction.

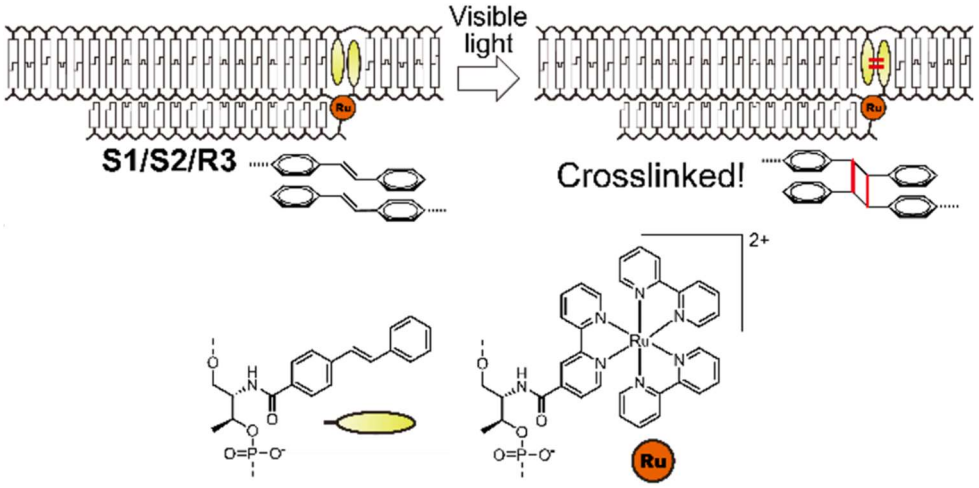

Figure 4-1. Schematic illustration of photo-crosslinking system mediated by $Ru(bpy)_3$.

4-4 Results and discussions

4-4-1 Effect of $Ru(bpy)_3$ on the structure of DNA triplexes

The [2+2] cycloaddition reaction of stilbenes is promoted by the formation of H-aggregates among stilbenes in the DNA duplex [16]. We first confirmed that stilbene residues formed an

aggregate in the context of DNA triplex in the presence of $Ru(bpy)_3$. Absorption spectra of DNA triplex with $Ru(bpy)_3$ and a stilbene pair (S1/S2/R1) and DNA triplex with $Ru(bpy)_3$ and a stilbene monomer (N1/S2/R3) were measured.

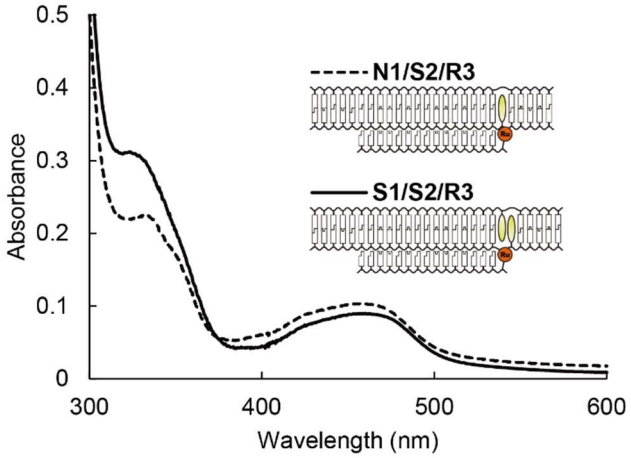

Figure 4-2. Absorption spectra of $Ru(bpy)_3$ and stilbene-introduced DNA triplexe.

Conditions

[DNA-Duplex] = 5.0 μM, [TFO] = 6.0 μM, [NaCl] = 100 mM

10 mM phosphate buffer, pH = 5.5, 20 °C

The UV/Vis spectrum of S1/S2/R1 showed a broad band at λ=320–380 nm with an absorption maximum at λ=324 nm (Fig. 4-2). The hypsochromic shift of this band in the spectrum of S1/S2/R1 with respect to that in the spectrum of N1/S2/R1 (λmax=334 nm) is characteristic of H-aggregate formation. Thus, it was indicated that $Ru(bpy)_3$ with large molecular size did not inhibit the stilbene residues aggregate formation in S1/S2/R1, a conformation that should allow photocycloaddition.

We next confirmed that the thermal stability of DNA triplexes is not destabilized in the presence of $Ru(bpy)_3$. Melting temperatures of DNA triplex with $Ru(bpy)_3$ (S1/S2/R3) and DNA duplex (S1/S2) were measured.

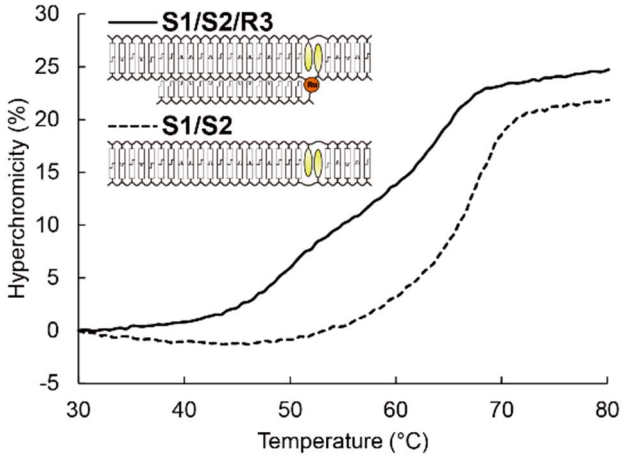

Figure 4-3. Melting profiles of the S1/S2/R3 triplex (solid line) and the S1/S2 duplex (broken line).

Conditions

[DNA-Duplex] = 1.0 μM, [TFO] = 1.2 μM, [NaCl] = 100 mM

10 mM phosphate buffer, pH = 5.5

The melting curves of S1/S2/R3 showed two-step transitions, indicating that DNA triplex can be formed even in the presence of $Ru(bpy)_3$ (Fig. 4-3). The melting temperatures for S1/S2/R1 were 51.0 and 67.0 °C and that for S1/S2 was 67.2 °C. The fact that there was no difference in the melting temperatures of S1/S2/R1 and S1/S2/ indicated that the introduction of the $Ru(bpy)_3$ did not destabilize the thermal stability of the DNA triplex.

4-4-1 Energy calculation

The emission of the $Ru(bpy)_3$ was observed from 550 nm to 700 nm (Fig. S4-1). This is far from the absorption region of stilbene (Fig. 4-2). Therefore, FRET from the $Ru(bpy)_3$ to stilbene cannot occur. The energy transfer from the $Ru(bpy)_3$ to the stilbene is thought to occur by triplet-triplet energy transfer (TTET). To verify if TTET from $Ru(bpy)_3$ to stilbene occurs, we evaluated the energy levels of the relevant excited states using quantum chemical calculations. The energy diagram of $Ru(bpy)_3$ and the stilbene monomer was calculated at the B3PW91 level using the LanL2DZ for $Ru(bpy)_3$ and 6-31+G(d,p) for H, C, N, O atoms

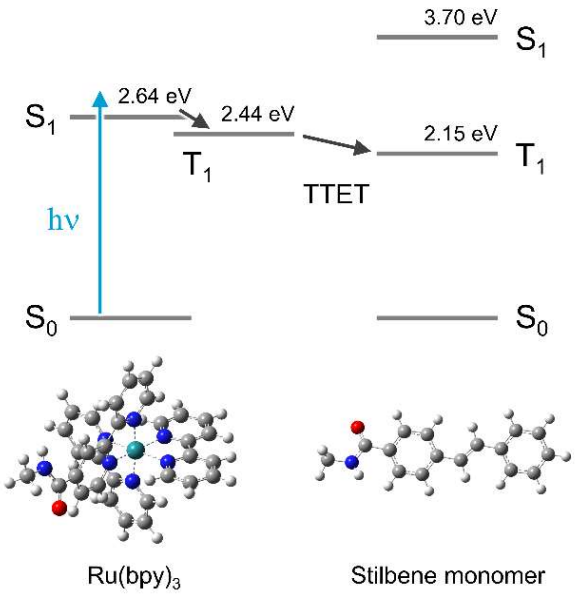

Figure 4-4. Energy diagram of $Ru(bpy)_3$ and stilbene monomer obtained from quantum chemical calculation. The D-threoninol backbone was replaced with a methyl group to reduce computational costs.

The triplet excited state energy of the $Ru(bpy)_3$ was calculated to be A 2.64 eV (470 nm), and that of the stilbene monomer was xalculated tobe 2.15 eV (335 nm) (Fig. 4-4). The absorption wavelengths predicted from the calculated energies are in good agreement with the experimentally observed absorption wavelengths. The triplet excited state energy of the $Ru(bpy)_3$ was slightly higher than that of the stilbene monomer, suggesting that TTET is the dominant energy transfer from the $Ru(bpy)_3$ to stilbene. Since TTET occurs in a Dexter mechanism with a very short donor-acceptor distance (< 1 nm)[17], a site-selective [2+2] cycloaddition reaction can be expected by using $Ru(bpy)_3$ and stilbene in DNA triplex.

4-4-2 Cross-linking one site of DNA duplex with visible light irradiation

We then irradiated S1/S2/R1 with visible light at λ=465 nm to investigate the [2+2] photocycloaddition reactivity of stilbene residues. DNA triplets were irradiated with a 465 nm LED Absorption spectrophotometry and HPLC analysis were performed to confirm the progress of the DNA duplex cross-linking reaction.

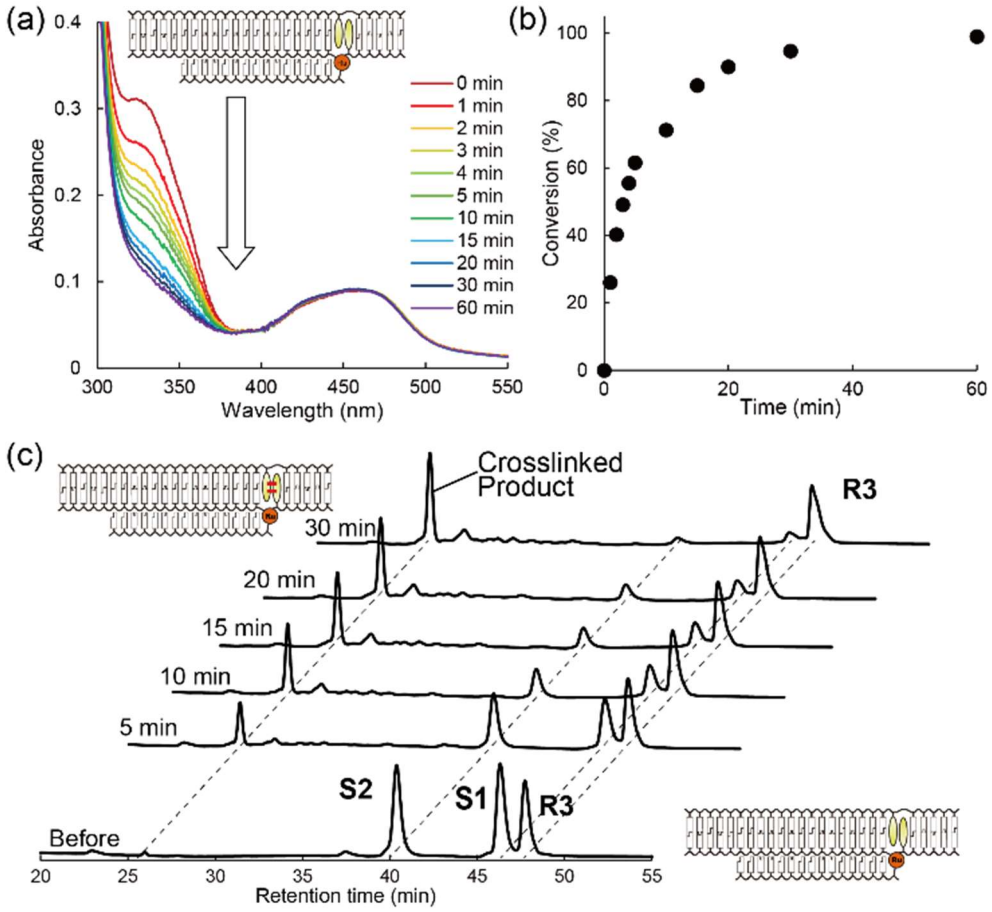

Figure 4-5. (a) Absorption spectra of S1/S2/R3 triplex before and after photoirradiation at 465 nm for the indicated duration. (b) Reaction kinetics determined from changes in absorption spectra. (c) HPLC chromatograms of the S1/S2/R3 triplex before and after photoirradiation at 465 nm for the indicated duration.

Conditions

[DNA-Duplex] = 5.0 μM, [TFO] = 6.0 μM, [NaCl] = 100 mM

10 mM phosphate buffer, pH = 5.5, 20 °C

Irradiation wavelength = 465 nm

The absorption band at λ=324 nm decreased with irradiation time and almost disappeared after 60 min of irradiation (Fig. 4-5a). This suggests that the progress of [2+2] photocycloaddition reactivity of stilbene residues. In contrast, almost no spectral changes were observed for the DNA triplex without $Ru(bpy)_3$ (S1/S2/N3) (Fig. S4-2) and the DNA triplex with only a stilbene (N1/S2/R3) (Fig. S4-3) upon photoirradiation. HPLC analysis suggested that the DNA duplexes were cross-linked by visible light irradiation. Before light irradiation, two peaks corresponding to S1 and S2 were observed. After light irradiation, these two peaks almost disappeared, and one new product peak appeared with a short retention time (Fig. 4-5c). These results suggest that the

$Ru(bpy)_3$ catalyzed the [2+2] cycloaddition of stilbene residues and cross-linked the DNA duplex.

To confirm that the product is the expected cross-linked DNA duplex, we investigated thermal stability of DNA. Melting temperatures of S1/S2/R3 before and after photoirradiation were measured.

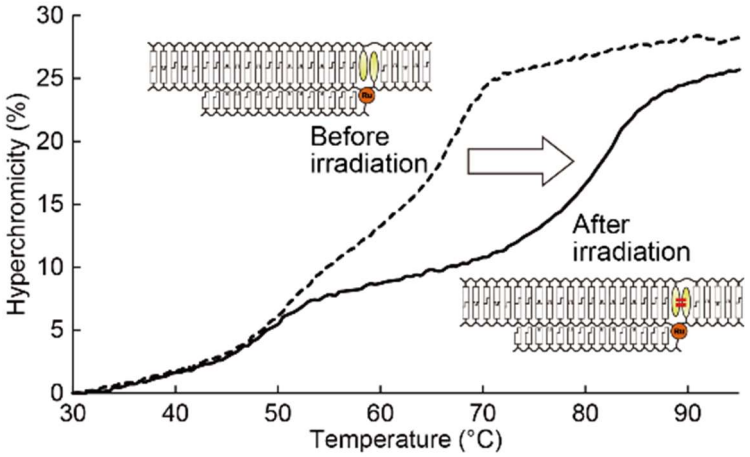

Figure 4-6. Melting profiles of S1/S2/R3 triplex before (broken line) and after (solid line) irradiation with 465 nm light for 30 min (solid line).

Conditions

[DNA-Duplex] = 1.0 μM, [TFO] = 1.2 μM, [NaCl] = 100 mM

10 mM phosphate buffer, pH = 5.5

The higher melting temperature of S1/S2/R3 before irradiation was 67.0 °C and after was 82.3 °C (Fig. 4-6). Melting measurements revealed that the melting temperature of the DNA duplexes increased after visible light irradiation, indicating an increase in thermal stability. Furthermore, the molecular weight of the product obtained from MALDI-TOF-MS analysis was consistent with the calculated value of the S1/S2 duplex (calculated mass = 16060.85, observed mass = 16092.93) (Fig. S4-4). From these results, we concluded that the product observed after visible light irradiation is a cross-linked DNA duplex by [2+2] cycloaddition of stilbenes by a $Ru(bpy)_3$.

On the other hand, the absorption band at λ=450 nm of the $Ru(bpy)_3$ remained unchanged after visible light irradiation (Fig. 4-6); in HPLC analysis (Fig. 4-6), there was no change in the peak of the $Ru(bpy)_3$-introduced DNA, and the molecular weight obtained from MALDI-TOF-MS analysis was consistent after visible light irradiation (calculated mass = 5171.86, observed mass = 5174.77). Furthermore, the lower melting temperature did not change before (51.0 °C) and after photoirradiation (49.4 °C). These results strongly suggest that the $Ru(bpy)_3$ introduced into the DNA is stable in this reaction.

To investigate the versatility of this system, a DNA triplex with stilbene and $Ru(bpy)_3$ on the opposite side of S1/S2/R3 (S8/S9/R4) was irradiated with visible light. Absorption spectra and melting temperatures were measured to confirm the progress of the reaction.

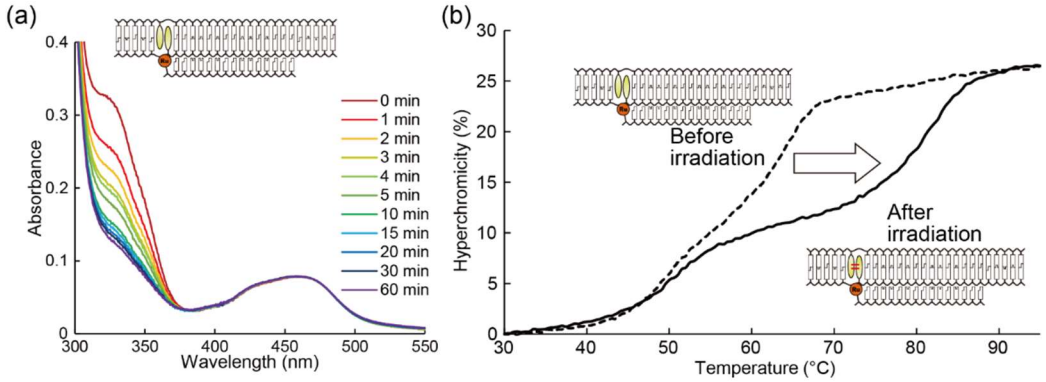

Figure 4-7. (a) Absorption spectra as a function of time and (b) melting profiles of S8/S9/R4 triplex before and after 30 min of photoirradiation.

Conditions

(absorption spectrum)

[DNA-Duplex] = 5.0 μM, [TFO] = 6.0 μM, [NaCl] = 100 mM

10 mM phosphate buffer, pH = 5.5, 20 °C

Irradiation wavelength = 465 nm

(melting temperature)

[DNA-Duplex] = 1.0 μM, [TFO] = 1.2 μM, [NaCl] = 100 mM

10 mM phosphate buffer, pH = 5.5

The absorbance of stilbene in S8/S9/R4 decreased as in S1/S2/R3 (Fig. 4-7a). The higher melting temperature of S7/S8/R4 before irradiation was 64.2 °C and after was 82.2 °C (Fig. 4-7b). These temperatures were comparable to S1/S2/R3, respectively. These results indicate that when stilbene and $Ru(bpy)_3$ are in close proximity, DNA duplexes can be cross-linked independently of the DNA sequence.

4-4-3 Site-selective cross-linking

Since energy is transferred from the $Ru(bpy)_3$ to the stilbene by TTET, site-selective cross-linking of DNA duplexes is expected. To confirm that the cross-linking of DNA duplexes can be controlled based on the position of the $Ru(bpy)_3$, we irradiated the triplex with the $Ru(bpy)_3$ introduced on the opposite side of the stilbene-introduced position (S1/S2/R4) and the TFO with duplex which do not form triplex (Sc1/Sc2 with R3) with visible light. Absorption spectra were

measured to verify the progress of the reaction.

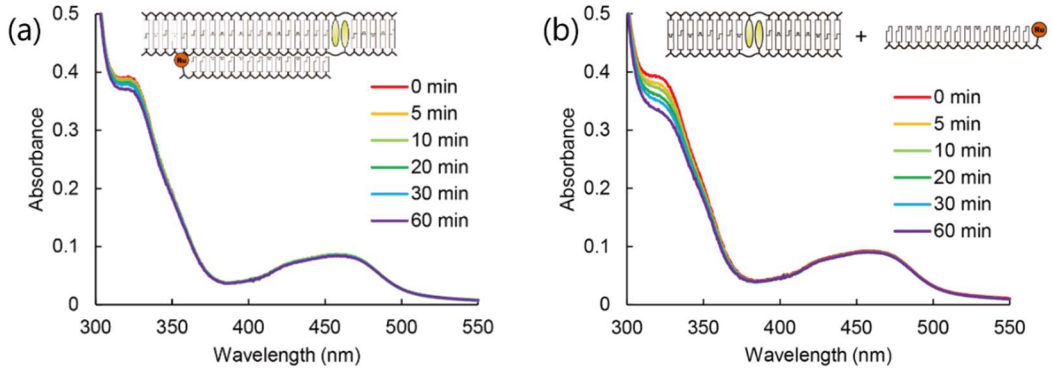

Figure 4-8. Absorption spectra of (a) the S1/S2/R4 and (b) Sc1/Sc2 with R3 before and after irradiation at 465 nm for the indicated durations.

Conditions

[DNA-Duplex] = 5.0 μM, [TFO] = 6.0 μM, [NaCl] = 100 mM

10 mM phosphate buffer, pH = 5.5, 20 °C

Irradiation wavelength = 465 nm

The absorbance of stilbene in S1/S2/R4 hardly decreased after irradiation with visible light (Fig. 4-8a). This indicates that the [2+2] cycloaddition of stilbene is not catalyzed by the $Ru(bpy)_3$ when the stilbene and $Ru(bpy)_3$ are separated in the DNA triplex. The absorbance of stilbene in Sc1/Sc2 with R3 decreased slightly and the rate of decrease was much slower than that in S1/S2/R3 after irradiation with visible light (Fig. 4-8b). This indicates that the intermolecular [2+2] cycloaddition of stilbene is hardly catalyzed by the $Ru(bpy)_3$ These results suggest that site-selective DNA duplexes can be cross-linked by designing the DNA sequence.

4-4-4 The phosphorescence lifetime of $Ru(bpy)_3$ was measured to verify TTET from $Ru(bpy)_3$ to stilbene.

The results of energy transfer calculations indicate that $Ru(bpy)_3$ can TTET to stilbene. Therefore, we measured the phosphorescence lifetime of $Ru(bpy)_3$ in N1/N2/R3 and S1/S2/R3 to verify the TTET from $Ru(bpy)_3$ to stilbene.

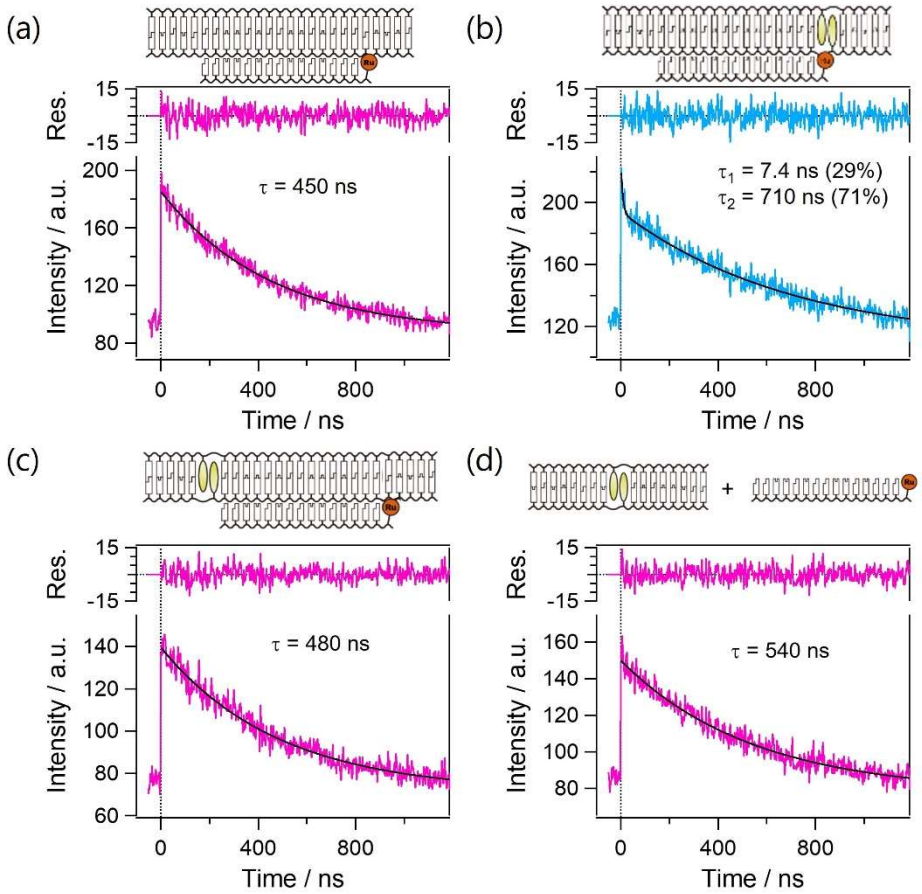

Figure 4-9. Phosphorescence decay curves of $Ru(bpy)_3$ in (a) N1/N2/R3), (b) S1/S2/R3, (c) S8/S9/R3 and (d) Sc1/Sc2 with R3. Calculated phosphorescence lifetimes and abundance ratios are also shown.

Conditions

[NaCl] = 100 mM ,10 mM phosphate buffer, pH = 5.5

Excitation wavelength = 440 nm, Emission wavelength = 620 nm

The phosphorescence lifetime of $Ru(bpy)_3$ in N1/N2/R3 was well fitted with one component and its phosphorescence lifetime was calculated to be 450 ns (Fig. 4-9a). The phosphorescence lifetime of $Ru(bpy)_3$ in S1/S2/R3 was well fitted by the two components, and their phosphorescence lifetimes were calculated to be 7.4 ns and 710 ns (Fig. 4-9b). The shorter phosphorescence lifetime of $Ru(bpy)_3$ in S1/S2/R3 was significantly shorter than the phosphorescence lifetime of $Ru(bpy)_3$ in N1/N2/R3. The phosphorescence lifetime of $Ru(bpy)_3$ was shortened when the stilbene pair and the $Ru(bpy)_3$ are in proximity, indicating TTET from $Ru(bpy)_3$ to stilbene. The longer phosphorescence lifetime of $Ru(bpy)_3$ in S1/S2/R3 was almost the same as the phosphorescence lifetime of $Ru(bpy)_3$ in N1/N2/R3. This suggests that there are $Ru(bpy)_3$ that do not TTET to stilbene, and that when stilbene and $Ru(bpy)_3$ bump into each other

with a certain probability, they TTET. In contrast, the phosphorescence lifetime of $Ru(bpy)_3$ in N1/N2/R3 and Sc1/Sc2 with R3 was well fitted with one component and its phosphorescence lifetime was calculated to be 480 ns (Fig. 4-9c) and 540 ns (Fig. 4-9d). These phosphorescence lifetimes of $Ru(bpy)_3$ in S1/S2/R3 were almost the same as the phosphorescence lifetime of $Ru(bpy)_3$ in N1/N2/R3. This indicates that long-range TTET within DNA triplex and intermolecular TTET do not occur.

4-4-5 Cross-linking two site of DNA duplex with visible light irradiation

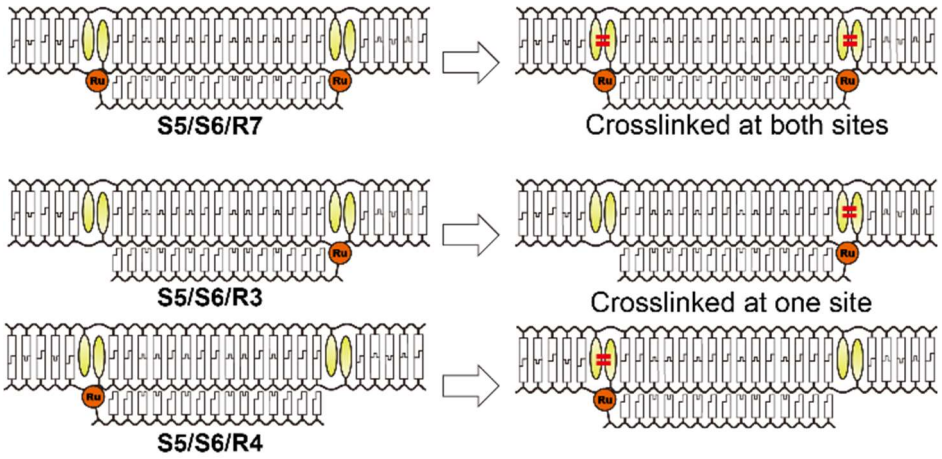

Figure 4-10. Schematic illustration of site-selective photo-crosslinking of DNA duplexes with two cross-linking positions.

We next attempted to control the cross-linking position of a DNA duplex (S5/S6) with two cross-linking positions. In the DNA triplex with TFO with $Ru(bpy)_3$ on both sides (S5/S6/S7), both stilbene pairs are in close proximity to the $Ru(bpy)_3$. Visible light irradiation causes [2+2] cycloaddition of both stilbene pairs, resulting in cross-linking of the two sites of the DNA duplex. In contrast, in the DNA triplex with TFO with $Ru(bpy)_3$ on only one side (S5/S6/R3 or S5/S6/R4), one of the stilbene pair is in close proximity to the $Ru(bpy)_3$. Visible light irradiation causes [2+2] cycloaddition of one of the stilbene pair, resulting in cross-linking of the one site of the DNA duplex. To verify this site-selective cross-linking of DNA duplexes, S5/S6/R7, S5/S6/R3 and S5/S6/R4 were irradiated with visible light. Absorption spectrophotometry and HPLC analysis were performed to confirm the progress of the reaction.

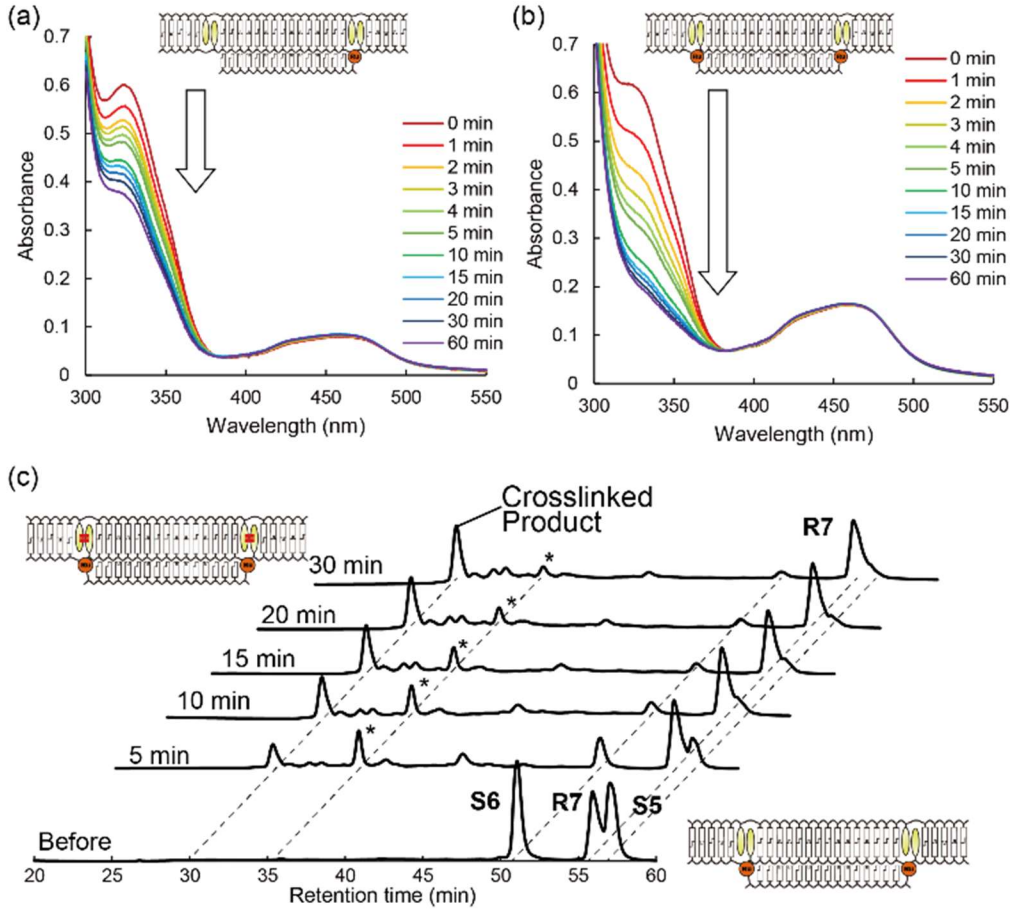

Figure 4-11. Absorption spectra of (a) S5/S6/R3 and (b) S5/S6/R7 triplexes. (c) HPLC chromatograms of the S5/S6/R7 triplex before and after photoirradiation at 465 nm for the indicated duration. The transient peak is indicated by an asterisk.

Conditions

[DNA-Duplex] = 5.0 μM, [TFO] = 6.0 μM

[NaCl] = 100 mM, 10 mM phosphate buffer, pH = 5.5, 20 °C

Irradiation wavelength = 465 nm

The absorbance of stilbene in S5/S6/R3 decreased with irradiation time, and about half of the absorbance remained after 60 minutes (Fig. 4-11a). This was also observed in S5/S6/R4 (Fig. S4-5a). These are different from S1/S2/R3 and S8/S9/R4. These results indicate that half of the stilbene were [2+2] cycloadducted in S5/S6 duplex. In contrast, the absorbance of stilbene in S5/S6/R7 decreased with irradiation time, and almost disappeared after 60 min of irradiation (Fig. 4-11b). This result indicates that all stilbenes were [2+2] cycloadducted in S5/S6. HPLC analysis showed that the S5 and S6 peaks observed before light irradiation almost disappeared after light irradiation, and new product peak was observed with short retention times (Fig. S4-6). This was also observed in S5/S6/R4 (Fig. S4-5c). The product peaks of S5/S6/R7 had shorter retention

times than that of S5/S6/R3 and S5/S6/R4 (Fig. 4-11c). Interestingly, a peak that was thought to be an intermediate appeared after 5 minutes and was observed to gradually disappear. This suggests that the S5/S6/R7 reaction proceeds in two steps.These results suggest that $Ru(bpy)_3$ selectively catalyze [2+2] cycloadditions of proximal stilbene pairs.

Melting temperatures were measured to verify site-selective DNA duplex cross-linking.

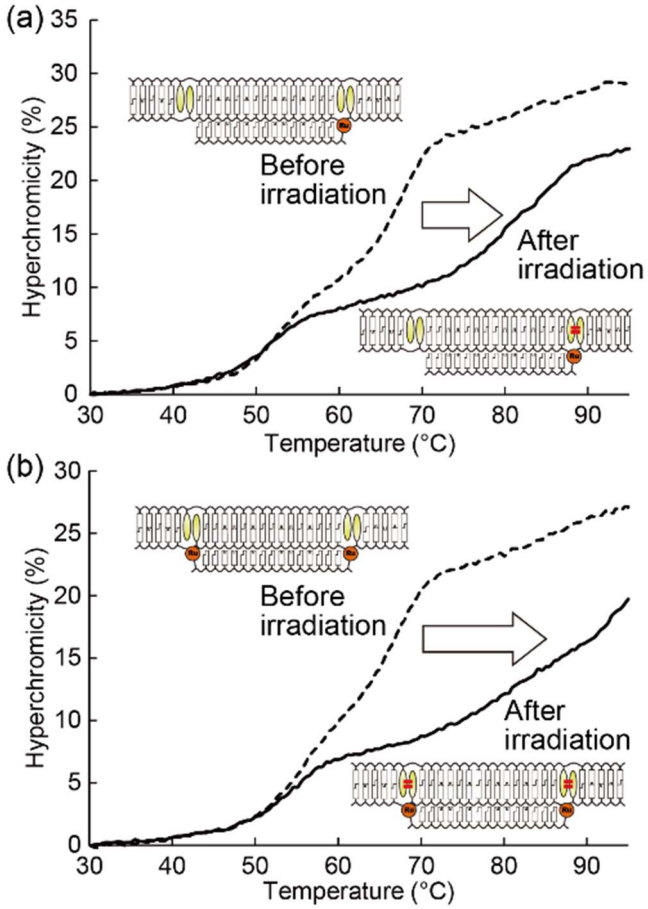

Figure 4-12. Melting profiles of (a) S5/S6/R3 and (b) S5/S6/R7 triplexes before and after photoirradiation at 465 nm for 30 min.

Conditions

[DNA-Duplex] = 1.0 μM, [TFO] =1.2 μM

[NaCl] = 100 mM, 10 mM phosphate buffer, pH = 5.5

The higher melting temperature of S5/S6/R3 before irradiation was 67.4 °C and after was 81.3 °C (Fig. 4-a). The higher melting temperature of S5/S6/R4 before irradiation was 67.1 °C and after was 83.9 °C (Fig. S4-5b). Their melting temperatures were similar to those of S1/S2/R3 and S8/S9/R4. These results indicate that irradiation of S5/S6/R3 and S5/S6/R4 with visible light selectively crosslinks one site of the S5/S6 duplex. In contrast, the higher melting temperature of

S5/S6/R7 before irradiation was 66.8 °C and after was >90 °C (Fig. 4-b). The melting temperature after visible light irradiation was higher than any previous melting temperature. This result indicates that irradiation of S5/S6/R7 with visible light crosslinks both sites of the S5/S6 duplex. From these results, we conclude that the photo cross-linking sites can be precisely controlled by changing the position of the $Ru(bpy)_3$ in the DNA triplex.

4-5 Conclusion

I In this study, we developed a novel cross-linking system for DNA duplexes by visible light irradiation. Visible light irradiation of a DNA triplex with a stilbene pair and $Ru(bpy)_3$ in close proximity catalyzed a [2+2] cycloaddition reaction of stilbene by $Ru(bpy)_3$, resulting in cross-linking of the DNA duplex. The introduction of $Ru(bpy)_3$ did not affect the structure of the DNA triplex. The energy calculations revealed TTET from $Ru(bpy)_3$ to stilbene. This cross-linking reaction was shown to be versatile, regardless of DNA sequence. It was shown that cross-linking of DNA duplexes can be controlled based on the position of $Ru(bpy)_3$ introduction and DNA sequence. It was shown to be able to selectively cross-link DNA duplexes that can be cross-linked at two sites based on the position of $Ru(bpy)_3$ introduction. The system does not require orthogonal photoreactive molecules, making it applicable to complex photoresponsive circuits and nanomachines.

4-6 Experimental section

Oligonucleotides

All conventional phosphoramidite monomers, CPG columns, reagents for DNA synthesis, and Poly-Pak II cartridges were purchased from Glen Research. Other reagents for the synthesis of phosphoramidite monomers were purchased from Tokyo Chemical Industry, Wako, and Aldrich. Native oligonucleotides were purchased from Integrated DNA Technologies. Modified oligomers were synthesized by employing modified phosphoramidite monomers and standard DNA monomers on an automated DNA synthesizer (M-6-MX, Nihon Techno Service). Oligomers were purified by reversed-phase HPLC and characterized by MALDI-TOF MS (Autoflex maX, Bruker) and HPLC.

Measurement of absorption spectra and melting temperatures

Absorption spectra were measured on a V-730 (JASCO). The sample solutions contained 100 mM NaCl, 10 mM phosphate buffer (pH 5.5), 5.0 μM DNA duplex, 6.0 μM TFO unless otherwise noted. Absorption spectra were measured at 20 °C after annealing at 80 ºC. The melting curves were measured with a UV-1800 (Shimadzu) by monitoring 260 nm absorbance versus temperature. The melting temperature (T_m) was determined from the maximum value and the second largest

value in the first derivative of the heating curve. The temperature ramp was 0.5 °C min-$^{1.}$ The sample solutions contained 100 mM NaCl, 10 mM phosphate buffer (pH 5.5), 1.0 μM DNA duplex, 1.2 μM TFO.

Emission measurements

Emission spectra were measured on JASCO model FP-8500. The excitation wavelength was 450 nm. Band widths were 2.5 nm for excitation and emission. Before measurements, sample solutions were heated at 80 °C, then slowly cooled to 20 °C at a rate of 1 °C min^{-1}. Emission spectra were measured at 20 °C. The sample solutions contained 100 mM NaCl, 10 mM phosphate buffer (pH 5.5), 1.2 μM DNA duplex, 1.0 μM TFO.

Photoirradiation

Light-emitting diodes (HLV2-22BL-3W, CCS Inc., 2.8 W) were used for photo-irradiation. The sample solution was added to a cuvette, and the temperature was controlled using a programmable temperature controller. The distance between the cuvette and the light source was set at 1.5 cm. No reflective setup was used for irradiation. Photoirradiation at 465 nm was conducted at 20 ºC. The sample solutions contained 100 mM NaCl, 10 mM phosphate buffer (pH 5.5), 5.0 μM DNA duplex, 6.0 μM TFO.

HPLC analyses

A Mightysil RP-18GP II column (Kanto Chemical Co., Inc.) heated to 65 °C was used for HPLC analyses. The flow rate was 0.5 mL min^{-1}. A solution of 50 mm ammonium formate (solution A) and 50 mm ammonium formate and acetonitrile (50:50, v/v; solution B) were used as mobile phases. A linear gradient of 5–25% solution B over 60 min was employed. Absorbance was monitored at 260 nm. Spectra of peaks at each retention time were recorded on JASCO EXTREMA HPLC system.

Quantum chemical calculation

Density functional theory (DFT) calculations were performed using the Gaussian 16 software package.[3] The molecular geometries of $Ru(bpy)_3$ and stilbene monomer were optimized at the B3PW91 level using the LanL2DZ for Ru and 6-31+G(d,p) basis set for H, C, N, O atoms. In the calculation, the D-threoninol backbone was replaced with a methyl group to reduce computational costs. No imaginary frequency was detected for the optimized structures. The electronic transition energies of the singlet and triplet states were calculated on the basis of time-dependent density functional theory (TD-DFT) with the same functional and basis sets.

4-7 References

1. Lerch, M. M.; Hansen, M. J.; Velema, W. A.; Szymanski, W.; Feringa, B. L., Orthogonal photoswitching in a multifunctional molecular system. *Nature Communications* **2016,** *7* (1), 12054.

2. Jeong, M.; Park, J.; Kwon, S., Molecular Switches and Motors Powered by Orthogonal Stimuli. *European Journal of Organic Chemistry* **2020,** *2020* (47), 7254-7283.

3. Lu, P.; Ahn, D.; Yunis, R.; Delafresnaye, L.; Corrigan, N.; Boyer, C.; Barner-Kowollik, C.; Page, Z. A., Wavelength-selective light-matter interactions in polymer science. *Matter* **2021,** *4* (7), 2172-2229.

4. Kamiya, Y.; Asanuma, H., Light-Driven DNA Nanomachine with a Photoresponsive Molecular Engine. *Accounts of Chemical Research* **2014,** *47* (6), 1663-1672.

5. Mayer, G.; Heckel, A., Biologically Active Molecules with a "Light Switch". *Angewandte Chemie International Edition* **2006,** *45* (30), 4900-4921.

6. Mukae, M.; Ihara, T.; Tabara, M.; Jyo, A., Anthracene–DNA conjugates as building blocks of designed DNA structures constructed by photochemical reactions. *Organic & Biomolecular Chemistry* **2009,** *7* (7), 1349-1354.

7. Fujimoto, K.; Matsuda, S.; Takahashi, N.; Saito, I., Template-Directed Photoreversible Ligation of Deoxyoligonucleotides via 5-Vinyldeoxyuridine. *Journal of the American Chemical Society* **2000,** *122* (23), 5646-5647.

8. Brieke, C.; Heckel, A., Spiropyran Photoswitches in the Context of DNA: Synthesis and Photochromic Properties. *Chemistry – A European Journal* **2013,** *19* (46), 15726-15734.

9. Ting, R.; Lermer, L.; Perrin, D. M., Triggering DNAzymes with Light: A Photoactive C8 Thioether-Linked Adenosine. *Journal of the American Chemical Society* **2004,** *126* (40), 12720-12721.

10. Doi, T.; Kawai, H.; Murayama, K.; Kashida, H.; Asanuma, H., Visible-Light-Triggered Cross-Linking of DNA Duplexes by Reversible [2+2] Photocycloaddition of Styrylpyrene. *Chemistry – A European Journal* **2016,** *22* (30), 10533-10538.

11. Yamano, Y.; Murayama, K.; Asanuma, H., Dual Crosslinking Photo-Switches for Orthogonal Photo-Control of Hybridization Between Serinol Nucleic Acid and RNA. *Chemistry – A European Journal* **2021,** *27* (14), 4599-4604.

12. Meade, T. J.; Kayyem, J. F., Electron Transfer through DNA: Site-Specific Modification of Duplex DNA with Ruthenium Donors and Acceptors. *Angewandte Chemie International Edition in English* **1995,** *34* (3), 352-354.

13. Hurley, D. J.; Tor, Y., Donor/Acceptor Interactions in Systematically Modified RuII−OsII Oligonucleotides. *Journal of the American Chemical Society* **2002,** *124* (44), 13231-

13241.
14. Le Gac, S.; Rickling, S.; Gerbaux, P.; Defrancq, E.; Moucheron, C.; Kirsch-De Mesmaeker, A., A Photoreactive Ruthenium(II) Complex Tethered to a Guanine-Containing Oligonucleotide: A Biomolecular Tool that Behaves as a "Seppuku Molecule". *Angewandte Chemie International Edition* **2009,** *48* (6), 1122-1125.
15. Ischay, M. A.; Anzovino, M. E.; Du, J.; Yoon, T. P., Efficient Visible Light Photocatalysis of [2+2] Enone Cycloadditions. *Journal of the American Chemical Society* **2008,** *130* (39), 12886-12887.
16. Doi, T.; Kashida, H.; Asanuma, H., Efficiency of [2 + 2] photodimerization of various stilbene derivatives within the DNA duplex scaffold. *Organic & Biomolecular Chemistry* **2015,** *13* (15), 4430-4437.
17. Dexter, D. L., A Theory of Sensitized Luminescence in Solids. *The Journal of Chemical Physics* **1953,** *21* (5), 836-850.

4-8 Appendixes

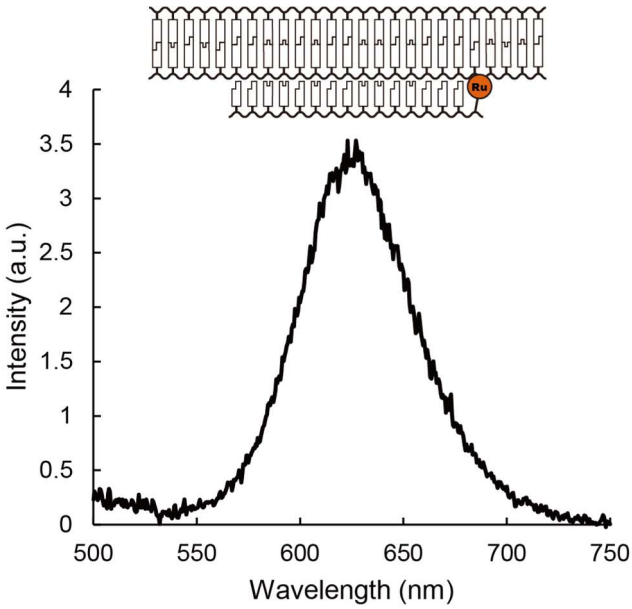

Figure S4-1. Phosphorescence emission spectrum of **N1**/**N2**/**R3** triplex. Excitation wavelength was 450 nm.

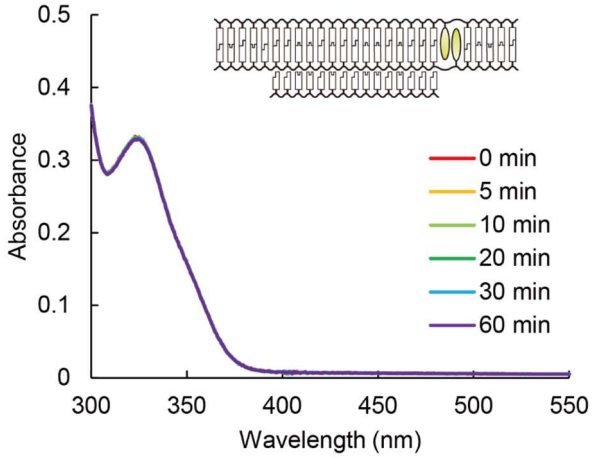

Figure S4-2. Absorption spectra of S1/S2/N3 triplex before and after photoirradiation at 465 nm for the indicated durations.

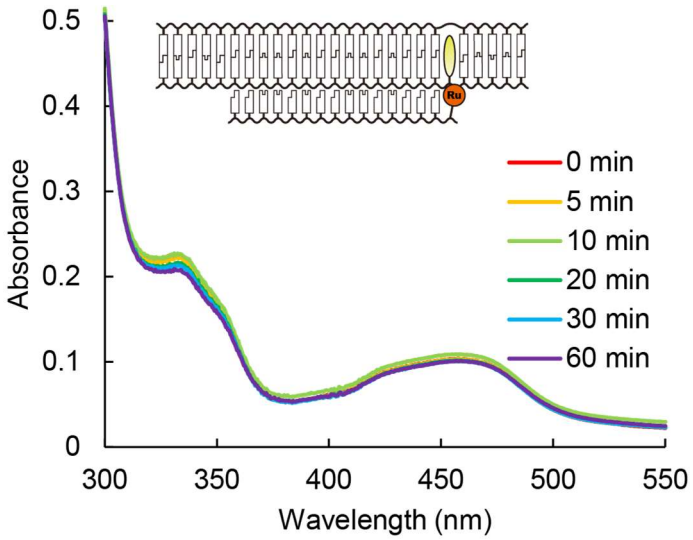

Figure S4-3. Absorption spectra of N1/S2/R3 triplex before and after photoirradiation at 465 nm for the indicated durations.

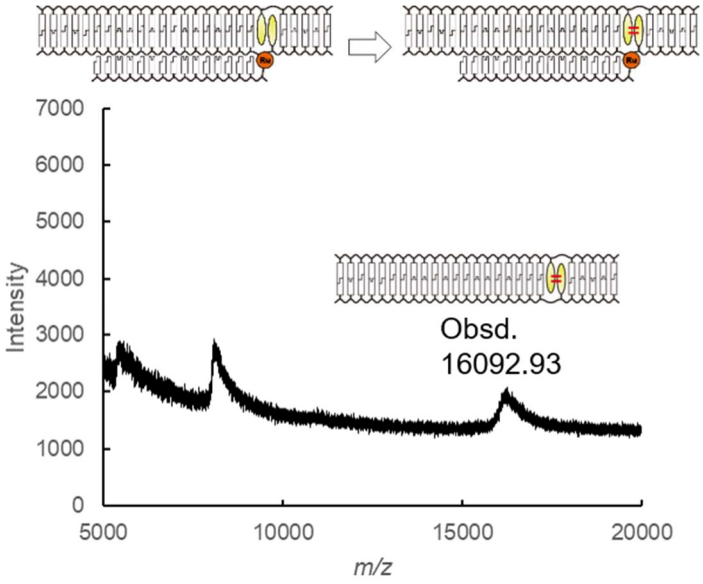

Figure S4-4. MALDI-TOF MS data of the crosslinked product of the S1/S2/R3 triplex after irradiation at 465 nm for 30 min. Calculated mass for crosslinked S1/S2 duplex is 16060.85.

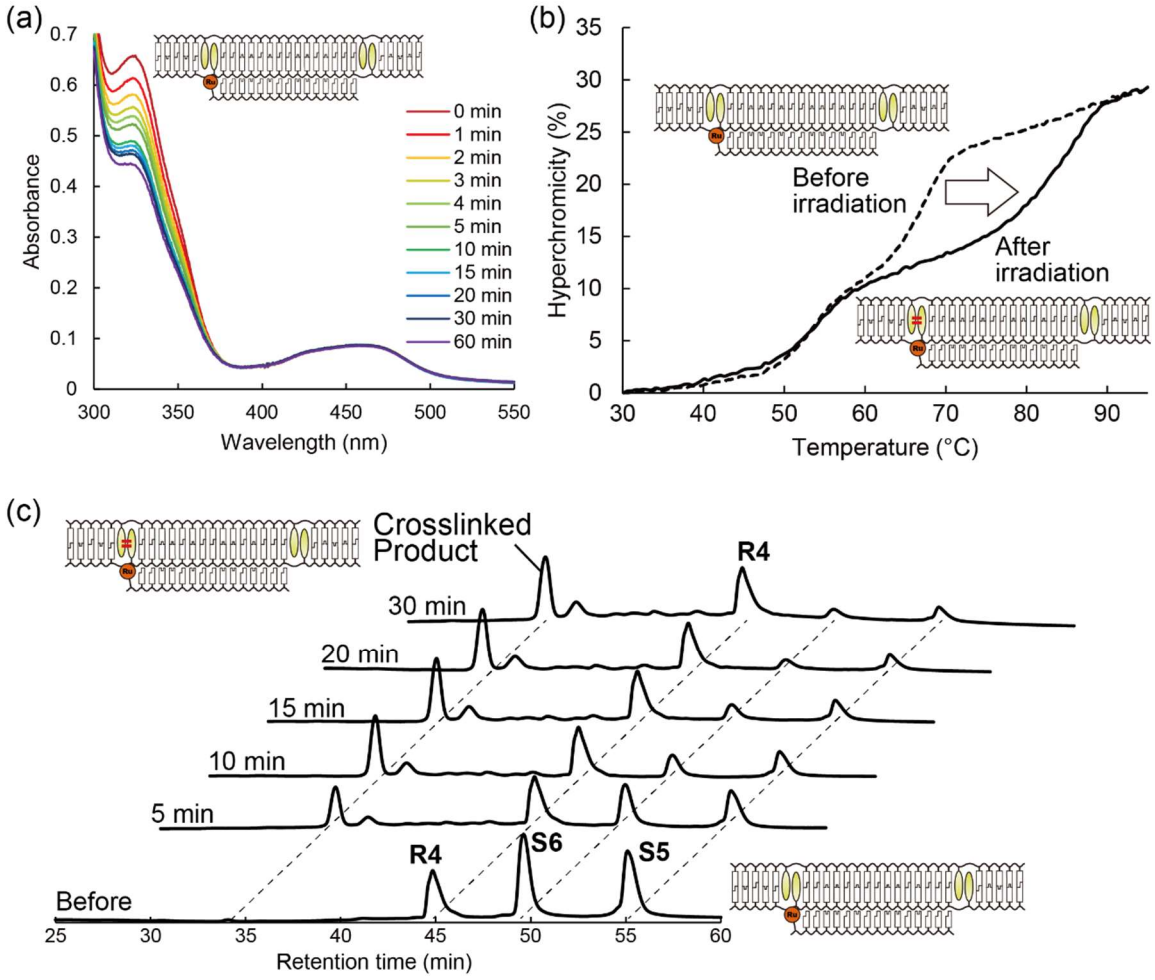

Figure S4-5. (a) Absorption spectra, (b) melting profiles, and (c) HPLC chromatograms of S5/S6/R4 triplex before and after photoirradiation. Irradiation time for absorption spectra and HPLC are indicated in the Figures. The melting profile was measured after irradiation for 30 min.

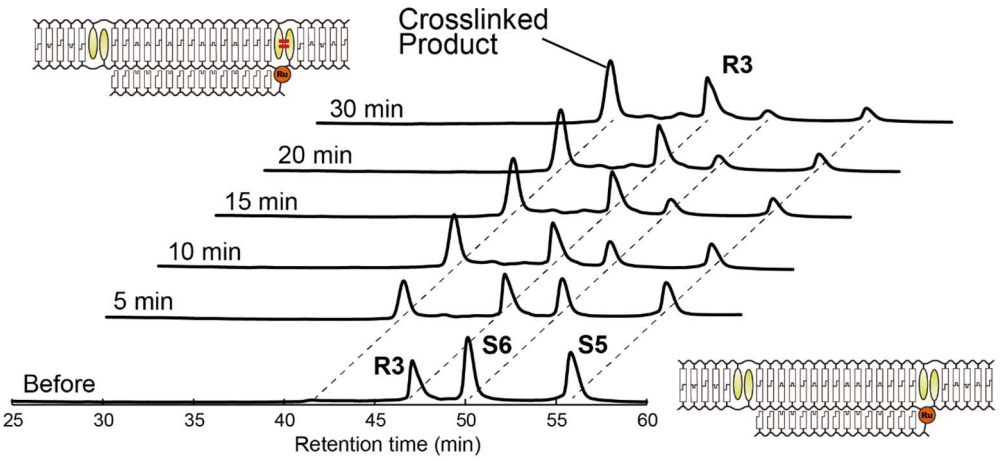

Figure S4-6. HPLC chromatograms of the S5/S6/R3 triplex before and after photoirradiation at 465 nm for the indicated durations.

Table S2-1 DNA sequence.

Name	Sequence (5'→3')
N1	AGTGATTCCTCTTCCTCTTTACGCT
N2	AGCGTAAAGAGGAAGAGGAATCACT
N3	TTTCTCCTTCTCCTT
S1	AGTGATTCCTCTTCCTCTTTStACGCT
S2	AGCGTStAAAGAGGAAGAGGAATCACT
S5	AGTGAStTTCCTCTTCCTCTTTStACGCT
S6	AGCGTStAAAGAGGAAGAGGAAStTCACT
S8	AGTGAStTTCCTCTTCCTCTTTACGCT
S9	AGCGTAAAGAGGAAGAGGAAStTCACT
Sc1	GTGCTATGStTCTCCGAA
Sc2	TTCGGAGAStCATAGCAC
R3	RuTTTCTCCTTCTCCTT
R4	TTTCTCCTTCTCCTTRu
R7	RuTTTCTCCTTCTCCTTRu

St: stilbene, Ru: $Ru(bpy)_3$

List of publications

1. Kashida, H.; Azuma, H.; Maruyama, R.; Araki, Y.; Wada, T.; Asanuma, H. "Efficient Light-harvesting Antenna Results from Densely Organizing Dyes into a DNA Junction via D-threoninol" *Angew. Chem. Int. Ed.*, **2020**, *59*, 11360-11363.

2. Kashida, H.; Azuma, H.; Sotome, H.; Miyasaka, H.; Asanuma, H. "Site-selective photo-crosslinking of stilbene pairs in a DNA duplex mediated by ruthenium photocatalyst" *Angew. Chem. Int. Ed.*, **2024**, *63*, e202319516.

List of presentations

International conference

Oral

1. Azuma, H.; Kashida, H.; Asanuma, H. " Development of light harvesting antenna using DNA with multiple fluorophores" 2021 International Chemical Congress of Pacific Basin Societies, December 17-22, Virtual, Session#110 (2021)

2. Azuma, H.; Asanuma, H.; Kashida, H. " Development of efficient light harvesting antenna using DNA junction with multiple fluorophores" 17th International Symposium on Macrocyclic and Supramolecular Chemistry, June 25-29, Reykjavik (Iceland), T2 (2023)

Internal conference

18 presentations. Omitted.

List of awards

1) 2018 年度 日本化学会東海支部長賞（卒論）

2) 卓越大学院 GTR プログラム 2019 年度成果報告会 GTR Poster Award

3) 2020 年度 東海高分子研究会優秀口頭発表賞

4) 2020 年度 名大鏡友会賞（修論）

Acknowledgement

The present article is a thesis for application of a doctoral degree at the Department of Biomolecular Engineering, Graduate School of Engineering, Nagoya University. All the study work was conducted under the direction of Professor Hiroyuki Asanuma from April 2018 to March 2024.

I would like to express my sincere gratitude to Prof. Hiroyuki Asanuma and Associate Professor Hiromu Kashida who provided a number of helpful comments and valuable suggestions which were necessary for improvement of this study.

I also especially thank Professor. Yukiko Kamiya (Kobe pharma Uviv.) and Assistant professor Keiji Murayama who provided a lot of comments for my investigation.

I would also like to say thanks for co-worker Dr. Koki Makino, Dr. Fuminori Sato, Ms. Hikari Okita, Mr. Keito Hirano, and other members of Asanuma Laboratory for their contribution to this study.

I would like to give special thanks to Professor Tsukasa Torimoto and Professor Kentaro Tanaka for giving helpful comments and suggestion on this thesis.

I would like to thank my parents and brother for their understanding and support.

Finally, I would like to thank my wife Ayano for her love and constant support.